Applied Catalysis B: Environmental 239 (2018) 485–501

Contents lists available at ScienceDirect

Applied Catalysis B: Environmental

journal homepage: www.elsevier.com/locate/apcatb

NO reduction by CO over copper catalyst supported on mixed CeO_2 and Fe_2O_3: Catalyst design and activity test

Xingxing Cheng*, Xingyu Zhang, Dexin Su, Zhiqiang Wang, Jingcai Chang, Chunyuan Ma*

National Engineering Lab for Coal-fired Pollutant Emission Reduction, School of Energy and Power Engineering, Shandong University, Jinan, 250061, China

ARTICLE INFO

Keywords:
NO reduction
CeO2
Catalyst
Carbon monoxide
Copper

ABSTRACT

Copper catalysts supported on co-synthesised Fe_2O_3 and CeO_2 mixed metal oxide support (Cu/CeO_2-Fe_2O_3, Cu/CF for short, CF as the support) were prepared for NO reduction by CO. Cu/CF catalysts showed better catalytic performance at 100–200 °C than samples of Cu/CeO_2 and Cu/Fe_2O_3 which were supported on single metal oxide. The interaction of Fe and Ce could enhance the catalytic activity. The catalysts were characterized by N_2 adsorption, TEM, XRD, Raman, XPS, H_2-TPR, EPR, and *in situ* DRIFT. Cubic CeO_2 was found to serve as the lattice framework in the support of mixed oxides. Fe_2O_3 phase are mainly formed on the surface of CeO_2 lattice in the CF involved samples, and the 'topped' Fe_2O_3 phase on the CeO_2 crystals may facilitate the incorporation of iron atoms into CeO_2 lattice. The high fraction of oxygen vacancy in catalyst Cu/CF may also facilitate the redox cycle of oxygen during catalytic reactions. The interaction of Cu oxide with CF support favourably promotes the reduction of Cu oxide and diffusion of surface oxygen species at low temperatures. During the NO + CO catalytic reactions, CeO_2 serves as the storing sites of carbonate and enhances CO oxidation, Fe_2O_3 serves as the storing sites of nitrites and nitrates and facilitates NO_x adsorption, and impregnated copper helps to convert inactive nitrites into active intermediates for NO + CO reaction. The promoted adsorption and conversion of both carbonates and nitrite/nitrates over catalyst Cu/CF could be the reason of its excellent catalytic activity for NO + CO reaction.

1. Introduction

NO_x abatement is receiving more attention due to the stringent environment regulations, especially for stationary emission sources. A promising method is catalytic NO reduction by CO, which has been extensively investigated in literature [1–4]. This technology is quite attractive for many stationary industrial applications such as steel and coking factories, where CO is readily available as a byproduct. However, up to now it hasn't been applied in industry since NO reduction efficiency is always significantly suppressed by the presence of excess oxygen in the flue gas [5–10]. In order to overcome the negative effect of oxygen, we proposed a rotary reactor by separating catalytic NO reduction into an adsorption zone and a reduction zone, and over 90% NO_x removal efficiency was achieved at 200–250 °C over activated coke based catalysts FeCo/ASC [11], and at 350–450 °C over zeolite catalysts Fe/ZSM-5 [12]. It was also indicated that the good catalytic activity for CO + NO reaction is critical for the excellent performance of NO_x removal in this NO_x adsorption-reduction process.

In the past decades metal oxide catalysts have been extensively studied for the catalytic reduction of NO by CO due to its high catalytic activity and low reaction temperature. Copper [13–17] and ion [18–21] based catalysts are the most extensively studied since they are cheap, easily available, and excellent for catalytic reactions. CuO supported on CeO_2 have been frequently reported for its outstanding catalytic performance and potential application for NH_3-SCR reaction [16,22], CO + NO reaction [23,24], CO oxidation [25,26], and complete oxidation of volatile organic compounds [27]. In principle, the high activity of CuO-CeO_2 is correlated with the synergism of copper-ceria interactions, which facilitates the electron exchanges between Cu^{2+}/Cu^{+} and Ce^{3+}/Ce^{4+}, with both components being significantly more readily reduced or oxidized than the corresponding independent ones [18,26].

Active components dispersed on mixed metal oxides often produce superior activity to those supported on single oxide for a number of reactions [28]. Attempts to obtain a cerium based mixed oxides support, in order to improve the catalytic behaviour, have been the objective of some very recent investigations [23,29]. Enormous studies on CeO_2 modified CuO based catalysts have been conducted by several research groups [18,26], and the addition of some other metal oxides into the CeO_2 support could greatly promote the activity of CO + NO

* Corresponding authors.
E-mail addresses: xcheng@sdu.edu.cn (X. Cheng), chym@sdu.edu.cn (C. Ma).

https://doi.org/10.1016/j.apcatb.2018.08.054
Received 4 April 2018; Received in revised form 24 July 2018; Accepted 20 August 2018
Available online 22 August 2018
0926-3373/

reactions. A series of ceria-based solid solutions ($Ce_{0.67}Zr_{0.33}O_2$, $Ce_{0.67}Sn_{0.33}O_2$, $Ce_{0.67}Ti_{0.33}O_2$) were synthesized by inverse co-precipitation, and then used as supports to prepare $CuO/Ce_{0.67}M_{0.33}O_2$ ($M = Zr^{4+}$, Sn^{4+}, Ti^{4+}) catalysts through wetness impregnation method [23]. The catalytic activity test suggested that the reduction of $CuO/Ce_{0.67}Zr_{0.33}O_2$ is easier than $CuO/Ce_{0.67}Sn_{0.33}O_2$ and $CuO/Ce_{0.67}Ti_{0.33}O_2$ catalysts, which may be attributed to the difference in the electronegativity of dopant. Different modification methods, co-impregnation and stepwise-impregnation method, have also been compared and results showed that the catalyst acquired by co-impregnation method exhibited stronger interaction owing to the more sufficient contact among each component of the catalysts, which is beneficial to the improvement of reduction behaviour [24]. *In situ* FT-IR was employed to investigate CO or/and NO interaction with CuO supported on $Ce_{0.67}Zr_{0.33}O_2$ catalysts [30]. Dispersed CuO species were concluded to be the main active components for this reaction. The catalysts showed different activities and selectivities at low and high temperatures, which should be results from the reduction of dispersed copper oxide species. NO reduction by CO reaction was further studied over a series of $CuO/Ce_xZr_{1-x}O_2$ catalysts with different Ce/Zr molar ratios to evaluate the correlation of their structural characteristics with catalytic performance [31]. It was concluded that the dispersion capacity of CuO on the $Ce_xZr_{1-x}O_2$ was influenced by the crystal structures of supports and the ceria-rich (pseudocubic t") phase could anchor and stabilize the copper species more effectively than the zirconia-rich (t) phase. The differences in the coordination environments and lattice strains of $CuO/Ce_xZr_{1-x}O_2$ were considered as a reason for the different synergistic interaction between copper and ceria support. Other metals could also be added as active component. Binary metal oxides $CuO\text{-}CoO_x$ supported on $Ce_{0.67}Zr_{0.33}O_2$ catalysts had been investigated and the addition of cobalt species was found to promote the reduction of dispersed copper oxides and improve the catalytic activity toward NO removal by CO [32]. For these catalysts, the effect of H_2O and/or SO_2 on the catalytic activity of NO + CO was seldom reported since the copper catalysts always show very poor H_2O and/or SO_2 resistance.

Iron was also reported to be doped into copper/ceria catalysts to improve the catalytic activity. The catalytic behaviour of an iron-promoted copper/ceria catalyst toward CO oxidation (preferential oxidation of CO in H_2 rich streams, CO-PROX) was compared to that of an unpromoted sample with the same copper loading. Iron addition significantly reduces the amount of H_2 oxidation sites, likely promoting copper dispersion, leading better CO selectivity [33]. It was observed that H_2O could inhibit the catalytic reactions for catalysts of Cu/CeO_2, promoted by Fe or not. At lower temperatures, H_2O inhibit CO conversion on Fe promoted catalyst more than on the reference Cu/CeO_2 catalyst, although the performance is restored more rapidly. Fe doped $CuO\text{-}Ce_{0.8}Zr_{0.2}O_2$ (Cu/CZ) catalysts were also synthesised and it was found that mass ratio of Fe/Cu played an important role in the catalytic performance of CO oxidation (CO-PROX) [34]. The catalytic performance of Cu/CZ was improved by the addition of Fe, which was attributed to the lattice distortion due to the entry of metal ions into CeO_2 lattice. The formation of more oxygen vacancies and Cu^+ species was also explained to be the reason of improved catalytic activity. But H_2O also significantly inhibited the catalytic performance over these catalysts. The inhibition effect of H_2O was attributed to the blockage of CO chemisorption sites [35,36].

The aim of the present work is to develop catalysts with high catalytic activity and yet possess a low temperature window and good water resistance. The active metal is copper while the supports are mixed oxides of CeO_2 and Fe_2O_3. All the selected metals are cheap and environmentally friendly. We also designed a facile and environmental-friendly synthesis protocol to eliminate any waste water produced during the catalyst preparation. The catalytic activity of NO + CO reaction will be tested, as well as the influence of H_2O and SO_2. The structure of the synthesised catalysts will be discussed following the catalyst characterization. The reaction mechanism will be further explored based on the reaction behaviours and *in situ* DRIFT study.

2. Experimental

2.1. Catalyst preparation

The mixed oxides of CeO_2 and Fe_2O_3 were prepared by co-precipitation method. Requisite amount of $Ce(NO_3)_3{\cdot}6H_2O$ as Ce source and $Fe(NO_3)_3{\cdot}9H_2O$ as Fe source (Ce:Fe molar ratio is 1:1) was dissolved into distilled water to form solution. After being stirred for 1 h, the solution was evaporated in air at 160 °C. The obtained powders were then calcinated in air at 550 °C for 3 h. The as-prepared CeO_2-Fe_2O_3 oxide supports were denoted as cf. Pure CeO_2 and Fe_2O_3 were also prepared by the same procedure for comparison. The Cu/S (S = CF, CeO_2, Fe_2O_3) catalysts were further prepared by wetness impregnation method. The prepared oxide supports were stirred in $Cu(NO_3)_2$ solution for 1 h and then evaporated in air at 160 °C. All the obtained powders were finally calcinated in air at 550 °C for 3 h. The supported copper catalysts were denoted as Cu_x/CF, where x stands for the designed weight percentage of Cu loading. Catalysts with single oxide CeO_2 and Fe_2O_3 support are named as Cu/CeO_2 and Cu/Fe_2O_3, respectively. The designed Cu loadings in both Cu/CeO_2 and Cu/Fe_2O_3 are 4 wt.%. The two samples were also physically mixed, named as MM (mechanical mixture), and tested in some experiments for comparison. It could be seen that no solid or liquid waste was produced in this synthesis process and no additional acid or ammonia are needed, making the process simple, economically favorable and environmentally friendly.

2.2. Catalytic activity test

The catalytic activity was conducted in a fixed bed reactor system. To be brief, the reactor system consisted of a stainless steel tubular reactor (12.7 mm I.D.), a gas supply system equipped with mass flow controllers, a furnace, a gas analysis unit (FTIR flue gas analyzer GASMET DX4000) and a data acquisition system. The modeled gas for the catalytic test consisted of 800 ppm NO, 1600 ppm CO, 100 ppm SO_2 and 10% H_2O, balanced by N_2 with a total flow rate of 500 ml/min. H_2O was introduced in the gas mixture by passing the gas stream through a bubble gas saturator at 60 °C. The bulk volume of the catalysts loaded was 1 ml to maintain a gas hourly space velocity (GHSV) of 30,000 h^{-1}. Before the catalytic test, the catalyst samples were pelletized and crushed down into powders with an average diameter of 250–380 μm. 3–5 runs were performed for each reaction condition and the errors were calculated to be within 5%.

2.3. Catalyst characterization

The catalysts were characterized by several methods for their physical and chemical properties: high resolution transmission electron microscope (HRTEM) using a JEM-2100 instrument at an acceleration voltage of 200 kV; nitrogen adsorption at 77.35 K for specific surface area and pore size distribution using Quantachrome Autosorb 1C; ICP-AES (OPTIMA 7000DV from Perkin Elmer) for fractions of metal loading; powder X-ray diffractometer (XRD, Rigaku Dmax/2400) for crystal structures with Cu Kα radiation at a scanning rate of 8°/min over the 2θ range of 10–80°; Raman scattering measurements (JY-HR800, 532 nm, 0.3 mw) for supplemental information of crystal structures; X-ray photoelectron spectroscopy (XPS, AXIS ULTRA^{DLD}) for chemical valance states of surface atoms with Al Kα radiation (hv = 1486.6 eV) at 150 W; H_2 temperature-programmed reduction (H_2-TPR) for reducibility of the prepared samples with 50 mg sample loaded and 10% H_2/He as reductant (He for pretreating at 200 °C for 1 h followed by cooling to room temperature, H_2/He mixture for heating at a heating rate of 10 °C/min). Surface copper dispersion was measured by dissociative N_2O adsorption following the procedure described in reference [37]. The turnover frequency (TOF, s^{-1}) of NO per copper

atom was then calculated by $TOF = \frac{F(L/s)/22.4(L/mol)\cdot C_{NO}\cdot X_{NO}(\%)}{M(g)\cdot W_{Cu}(wt.\%)\cdot D_{Cu}(\%)/64(g/mol)}$, where, F is the flow rate of modeled flue gas, C_{NO} is the initial concentration of NO at the inlet, X_{NO} is NO conversion, M is the weight of catalysts loaded in each run, W_{NO} is the weight fraction of Cu loaded on the catalysts determined by ICP, and D_{Cu} is the copper dispersion determined by dissociative N_2O adsorption.

In situ diffuse reflectance infrared Fourier transform spectra (*in situ* DRIFT) was conducted for the analysis of reaction mechanism on a Nicolet 6700 FTIR spectrophotometer. 25 mg samples were first pretreated by an Ar stream at 400 °C for 1 h, and then cooled down to room temperature. Then a controlled stream of CO-Ar (5000 ppm) and/or NO-Ar (5000 ppm) at a rate of 100 ml/min for 40 min was fed into the sample chamber while the spectra were collected from 650 cm^{-1} to 4000 cm^{-1} at a spectral resolution of 4 cm^{-1} at various target temperature by subtraction of the corresponding background reference.

3. Results and discussion

3.1. Catalytic activity

The results of catalytic activity of different catalyst samples were presented in Fig. 1. Cu_4/CF exhibits the best catalytic performance, with a NO conversion of over 95% at 150 °C. On the contrary, support CF shows the worst catalytic activity, with negligible NO conversions below 150 °C and less than 50% conversion even at 200 °C. It's implied that active components on Cu_4/CF are mainly copper oxides, instead of the dominant support Fe_2O_3 and CeO_2. Copper oxide catalyst, when supported on single metal oxides Fe_2O_3 or CeO_2, presents worse activity than Cu_4/cf. Thus the synthesised mixed oxides in Cu_4/CF could significantly improve the catalytic performance of copper oxide. This effect is definitely caused by the interaction between closely contacting Fe and Ce species in Cu_4/CF since the mechanical mixture didn't exhibit any enhancement of catalytic activity (results not shown here).

NO could be reduced by CO into N_2O and/or N_2. No other observable N containing reduction products were detected in the experiments. Thus the N_2 selectivity could be calculated by $N_2 selectivity = 100\% - \frac{2\times[N_2O]_{out}}{[NO]_{in}-[NO]_{out}}$ with results shown in Fig. 1(b). For all the catalysts, N_2 selectivity increases with temperature since higher temperature is favourable for the further reduction of NO. Almost no N_2 selectivity could be observed at below 125 °C. Then the production of N_2 increases quickly at above 150 °C. Catalysts that show better catalytic performance in Fig. 1(a) also exhibit better N_2 selectivity, following an order of Cu_4/CF > Cu/CeO_2 > Cu/Fe_2O_3 > cf. Cu_4/CF catalyst shows the best N_2 selectivity among all the catalysts. But the selectivity is still very low at below 125 °C. It could increase to 90% at 200 °C, indicating that NO could be completely reduced into N_2 at above 200 °C. It have been widely recognized that the NO reduction mechanism is different at below and above 200 °C or 250 °C [23,30]. N_2O is the intermediate and product of NO + CO reaction at lower temperatures while N_2 tends to be the direct product at higher temperatures. Similar trend could also be observed over Cu/Fe_2O_3 and Cu/CeO_2, but at lower values.

The catalytic activity was also compared among Cu_x/CF catalysts with different copper loadings, as shown in Fig. 1(c) for NO conversion and Fig. 1(d) for N_2 selectivity. Both NO conversion and N_2 selectivity increase with copper loading with the best performance presented by Cu_4/cf. The effect of copper loading on catalytic activity could also confirm the previous speculation that copper is the main active component in the catalysts and copper oxides serve as active site during catalytic NO + CO reaction. The enhancement of the catalytic activity tends to be minor as copper loading is further increased from 2% (Cu_2/CF) to 4% (Cu_4/CF), which could be caused by the aggregation of metal oxides at higher loadings [38]. Further increasing of copper loading would decrease both NO conversion and N_2 selectivity due to metal aggregation, as indicated by the activity tests at higher copper loadings provided in the supplementary information (section S1).

The turnover frequencies (TOFs) of NO reaction over copper sites were also calculated with the results shown in Figs. 1(e) and (f), based on the copper dispersion data determined by dissociative N_2O adsorption in Table 1. It's quite clear that the promoting effect of supports for NO reduction over the active copper sites follows the order: CF > CeO_2 > Fe_2O_3. By comparing the TOFs of catalysts with different copper loading, it could be concluded that higher copper loading could affect the well dispersion of active metal sites and thus decrease the TOFs, although better NO conversion efficiencies are observed.

3.2. Physical properties (N_2 physisorption, TEM, XRD and Raman)

3.2.1. N_2 physisorption

The pore size distribution and surface area of the catalysts were tested by N_2 physical adsorption. Fig. 2(a) shows the N_2 adsorption-desorption profiles. All the catalysts present type III isotherm curves, indicating the presence of a wide range of pores, especially mesopores. The pore size distributions were calculated by BJH method with the results shown in Fig. 2(b). It could be observed that the pore diameters of all the catalysts are at around 10–40 nm, indicating a dominating existence of mesopores. Cu/CeO_2 catalyst has more micropores than other catalysts, and the peak is at around 13 nm, smaller than other catalysts. Cu/Fe_2O_3 catalyst has the smallest pore volume and the bigger peak pore size, 40 nm. Cu_x/CF catalysts with all copper loadings exhibit similar pore size distribution, with a maximum at about 20 nm, implying that the structure of the Cu_x/CF catalysts is determined by the same CF support. Impregnated copper could hardly affect the pore distribution due to its low loading rate. The pore volume of Cu_x/CF catalysts is between that of Cu/CeO_2 and Cu/Fe_2O_3, indicating both CeO_2 and Fe_2O_3 could contribute to the structure of CF support. The profiles of Cu_x/CF are similar with that of Cu/CeO_2, with similar trend and peak position. It is speculated that the texture structure of CF support is similar with CeO_2 instead of Fe_2O_3, although the designed molar ratio of Fe:Ce is 1.

The surface areas are calculated by BET method and presented in Table 1, together with total pore volume and average pore diameter. Cu/CeO_2 catalyst exhibits the highest surface area and total pore volume, and the smallest average pore diameter. Cu/Fe_2O_3 catalyst has the lowest surface area and total pore volume, and the biggest average pore diameter. Cu/CF catalysts, together with the bare support CF, have similar surface areas, total pore volumes, and average pore size. Copper loading rate has little effect on surface area and pore volume, implying that the low impregnation of copper didn't block the pores in the catalysts. The data agrees well with the discussions of Fig. 2.

3.2.2. TEM

The morphology of the catalysts with different supports was then investigated by TEM images in Fig. 3. Over Cu/Fe_2O_3 catalyst in Fig. 3(a), amorphous-shaped clusters could be observed with a size range of 35–70 nm and average value of 58 nm. The big crystalline size and resulted small pore volume confirms the results of N_2 physisorption study. In the HRTEM image with higher magnification in Fig. 3(b), crystal spaces were measured to be 0.29 nm, 0.26 nm, and 0.36 nm, which could be ascribed to the (104), (110) and (012) planes of hematite Fe_2O_3, respectively. Some impregnated copper could be observed as amorphous surface CuO_x at the edge of Fe_2O_3 crystals. The existence of CuO_x could be further confirmed by the TEM- Energy-dispersive X-ray spectroscopy (EDX) results provided in the supplementary information (Fig. S2).

In Fig. 3(c), wormhole-like mesostructure, aggregated by metal oxide nanoparticles, can directly be observed over samples Cu/CeO_2. Particle sizes of Cu/CeO_2 are around 6–17 nm with an average of 12.5 nm. Structural details of nanoparticles were obtained by HRTEM images in Fig. 3(d). Cu/CeO_2 sample exhibits spacing of lattice fringes around 0.31 nm, ascribed to the (111) crystallographic planes of CeO_2.

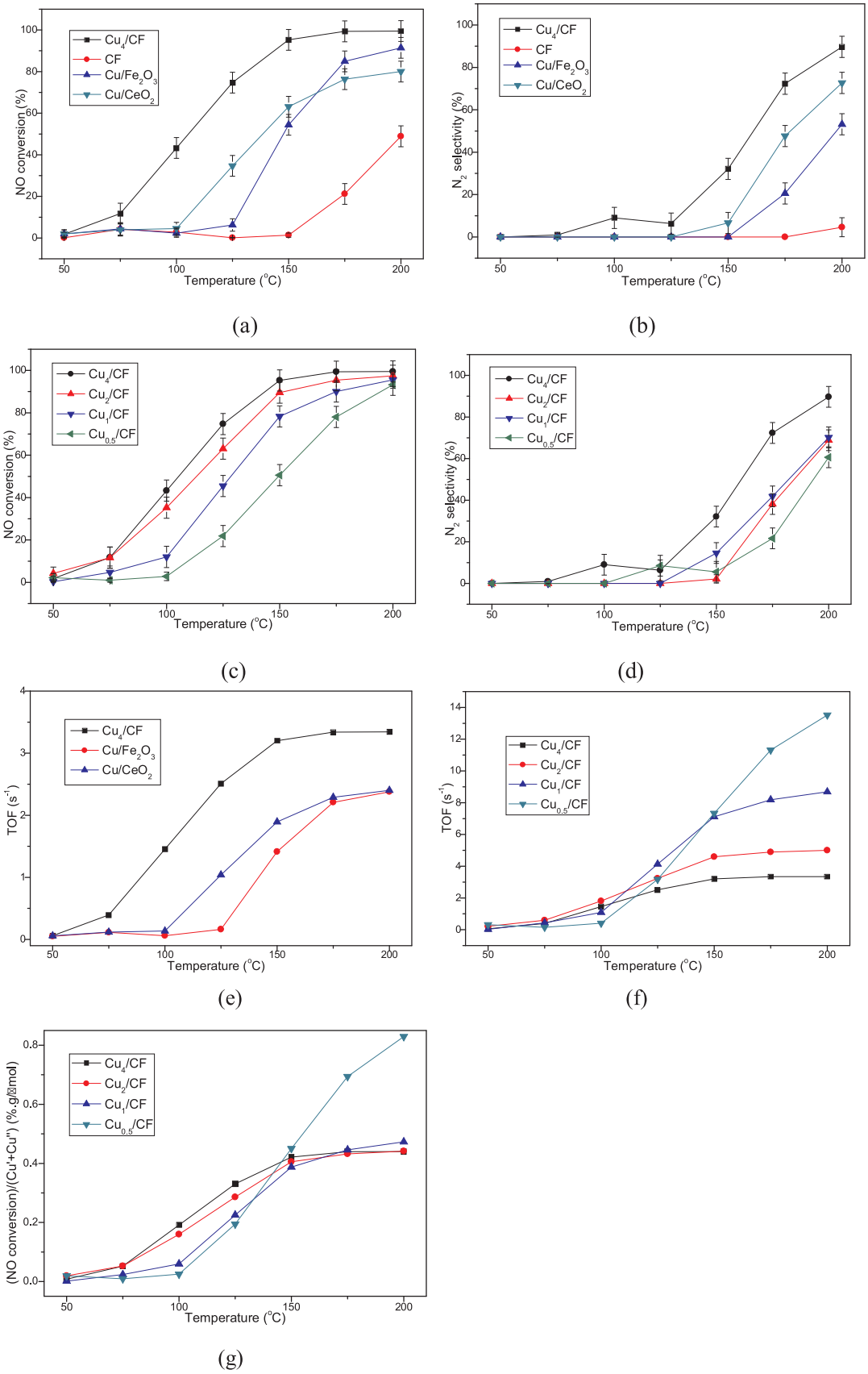

Fig. 1. Catalytic activity. a), NO conversion of catalysts with different supports; b), N_2 selectivity of catalysts with different supports; c), NO conversion of Cu_x/CF; d), N_2 selectivity of Cu_x/CF; e), TOF of catalysts with different supports; f), TOF of Cu_x/CF; g), (NO conversion)/(Cu'+Cu''). (Reaction condition: initial NO = 800 ppm, NO:CO = 1:2, GHSV = 30,000 h^{-1}).

Table 1
Properties of the catalysts.

Property	CF	Cu/Fe	Cu/Ce	Cu_4/CF	Cu_2/CF	Cu_1/CF	$Cu_{0.5}$/CF
S_{BET}(m^2/g)	41.48	12.60	56.05	41.89	41.58	45.27	41.28
V (cm^3/g)	0.183	0.103	0.213	0.177	0.195	0.180	0.174
d (nm)	18.68	33.61	13.16	17.42	17.44	17.41	17.45
Cu (wt.%)	/	3.65	3.77	3.55	1.72	0.87	0.53
Fe/Ce ratio	0.92	/	/	1.14	1.05	1.03	1.06
Cu dispersion (%)	/	40.05	33.80	31.96	43.15	48.18	49.58

S_{BET}, surface area determined by BET method.
d, average pore diameter determined by BJH method.
V, pore volume.
Cu, Cu content (wt.%) determined by ICP.
Fe/Ce ratio, molar ratio determined by ICP.
Cu dispersion, copper dispersion determined by dissociative N_2O adsorption.

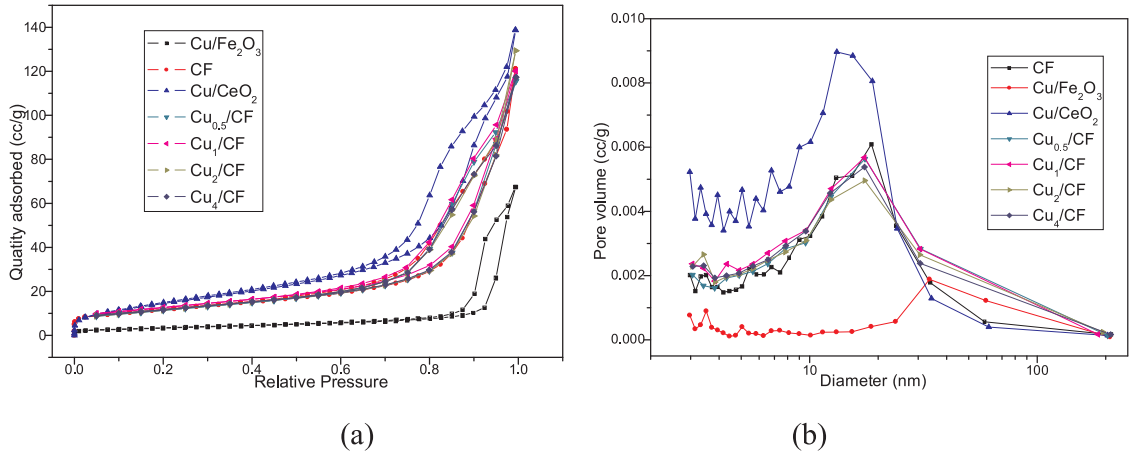

Fig. 2. Characterization of N_2 physisorption. (a) N_2 physisorption isotherm; (b) pore distribution.

A few CuO crystallites with the lattice spacing 0.21 nm, attributed to (111) plane of CuO, could also be observed at the edge of CeO_2 crystals. The existence of CuO could also be evidenced by TEM-EDX results in the supplementary information (Fig. S2).

In Fig. 3(e), similar wormhole-like mesostructure could be observed over sample Cu_4/CF like sample Cu/CeO_2, implying that the structure of CF support is similar with CeO_2 crystals. Particle sizes of Cu_4/CF are measured to be around 6–19 nm with an average of 11 nm, similar with those of Cu/CeO_2. The periodic fringes of 0.31–0.36 nm can be detected in HRTEM image in Fig. 3(f), which is compatible with the distance expected for (111) planes of CeO_2 lattice. Thus the lattice structure of the mixed metal oxide support CF is similar with CeO_2 instead of Fe_2O_3. Small amount of crystal Fe_2O_3 could be identified between the large CeO_2 crystals. Since the loaded atomic ratio of Fe:Ce is 1, it is speculated that some iron atoms are incorporated into the CeO_2 lattices. Cubic CeO_2 may serve as the lattice framework in the mixed oxides cf. As evidenced by EDX mapping profiles in the supplementary information (Fig. S3), the loaded Fe and Ce are not quite homogenous. But significant amount of Fe and Ce overlapping could also be observed, indicating the possibility of Fe incorporation into Ce lattice. In addition, some amorphous surface CuO_x, which are distributed on the top or at the edge of ceria crystal, are found over Cu_4/CF samples. A few CuO crystallites with a lattice spacing of 0.25 nm, attributed to ($\bar{1}$11) plane of CuO, could also be detected at the edge of CeO_2 crystals. It could be observed from Fig. S3 of the supplementary information that Cu seems well dispersed over the support. It could then be interpreted that significant amount of Cu is well dispersed over the CF support or impregnated in the support lattice, and is invisible from the TEM images. At the same time, a few aggregated CuO crystallites or amorphous surface CuO_x could be detected at the edge of CeO_2 crystals. Similar explanations could also be applied for samples Cu/Fe_2O_3 and Cu/CeO_2 over which only very few CuO crystals could be observed at the edge of support lattice.

3.2.3. XRD

The XRD diagram was then tested to identify the crystal phase on the catalysts as shown in Fig. 4(a). Over Cu/Fe_2O_3 sample, planes (012), (104), (110), (113), (024), (116), (214) and (300) of Fe_2O_3 (PDF# 33-0664) could be observed at 24.1°, 33.2°. 35.6°, 40.9°, 49.5°, 54.1°, 62.4°, and 64.0°, respectively. Thus the oxide support is mainly Fe_2O_3. Plane ($\bar{1}$11) of CuO (PDF#45-0937) could also be observed at 35.5°. No other peaks of CuO could be observed. Over Cu/CeO_2 catalyst, planes (111), (200), (220), (311), (222), (400), (331), (420), and (422) of cubic CeO_2 (fluorite structure, PDF#34-0394) could be observed at 28.6°, 33.1°, 47.5°, 56.3°, 59.1°, 69.4°, 76.7°, 79.1°, and 88.4°, respectively. CuO could not be detected in the XRD pattern. It is speculated that CuO loading is low and highly dispersed over the catalyst surface, making their peaks invisible over catalysts Cu/Fe_2O_3 and Cu/CeO_2. When Cu/Fe_2O_3 and Cu/CeO_2 are mixed (sample MM), CuO could still be hardly observed by XRD. Peaks of both CeO_2 and Fe_2O_3 could be detected while peaks of CeO_2 exhibit higher intensities. From the TEM images in Fig. 3(a) and (c), Fe_2O_3 is more amorphous while CeO_2 tends to form uniform crystals. This explains why CeO_2 present stronger XRD peaks. When Fe_2O_3 and CeO_2 are co-synthesised, the observed XRD pattern of the prepared CF sample is similar with that of sample MM, presenting the peaks of both Fe_2O_3 and CeO_2. It's again very obvious that peaks of CeO_2 are much stronger than Fe_2O_3. But the peaks of CeO_2 lattice on CF sample, taking the (111) plane for example, are much smaller than those on the solid mix sample MM, implying the strong interaction of CeO_2 and Fe_2O_3 lattice in the co-synthesised CF

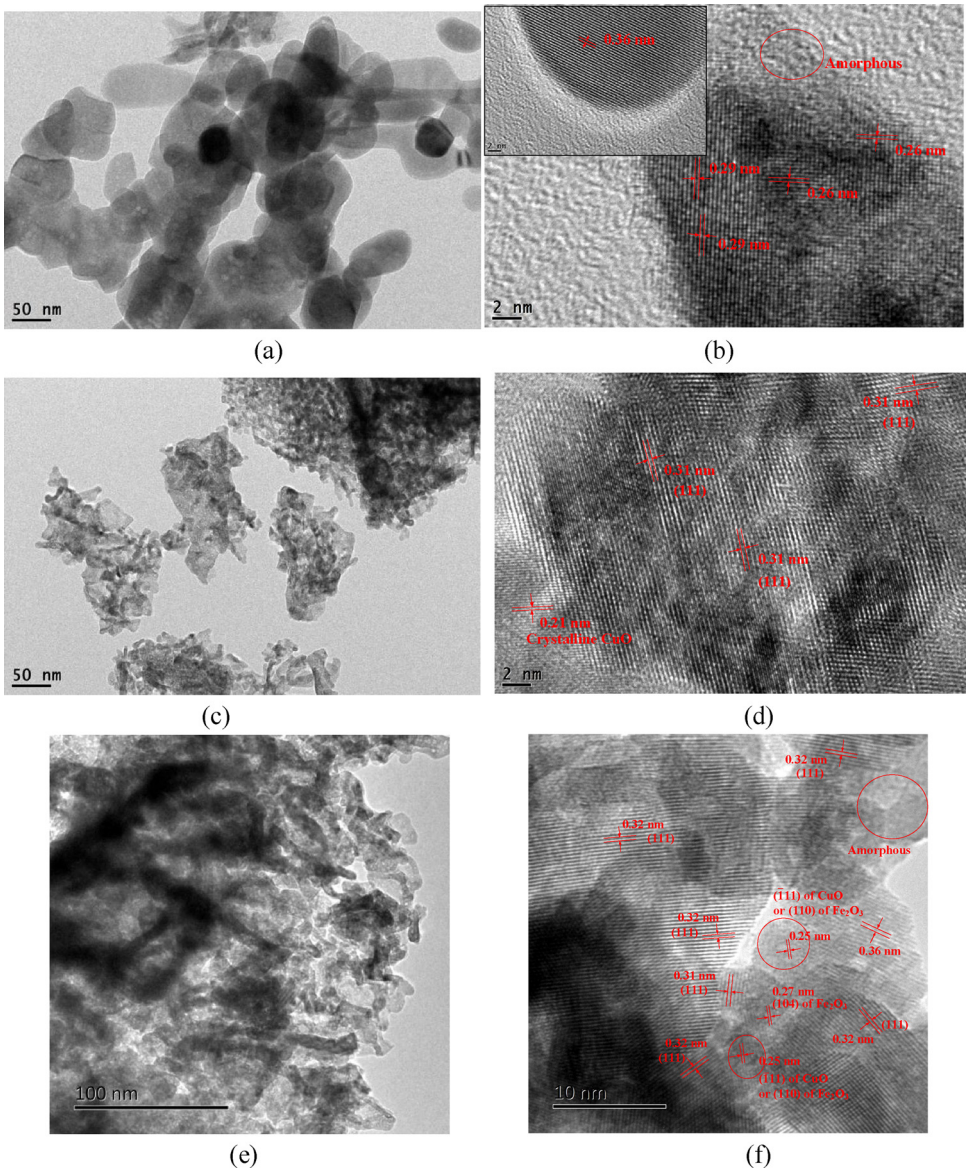

Fig. 3. TEM and HRTEM images of catalysts with different supports. a) and b), Cu/Fe_2O_3; c) and d), Cu/CeO_2; e) and f), Cu_4/cf.

sample. As evidenced in the magnified view of the main peak, the position of (111) plane left-shifts by 0.12° after Fe doping when comparing samples Cu/CeO_2 and cf. The deviation could be caused by CeO_2 lattice deformation due to Fe incorporation.

Similar XRD patterns could be observed over catalysts Cu_x/CF with different copper loadings and the same supports since the supporting oxides dominate the XRD peaks. Planes ($\bar{1}11$) and (111) of CuO could be detected at 35.5° and 38.7°, respectively. CuO oxides are highly dispersed over the CF support, indicated by the extremely small peak of CuO. When the Cu loading is lower than 1%, the peaks of CuO are invisible, implying a high dispersion of CuO phase. As Cu loading increased, peaks of CuO (111) plane increase correspondingly, indicating the appearance of aggregated CuO clusters. For the Cu_x/CF samples, peaks of both CeO_2 and Fe_2O_3 could be detected in the XRD diagram, indicating that the synthesized crystal phases are mainly Fe_2O_3 and CeO_2. Peaks of CeO_2 show apparently stronger intensities than those of Fe_2O_3. Similar XRD peaks of CeO_2 and Fe_2O_3 could also be observed for all the Cu_x/CF catalysts in Fig. 4(b). The weaker peaks of Fe_2O_3 could be caused by the amorphous phase of oxides like solid mix, or it could also be caused by the high dispersion of Fe_2O_3. In Fig. 3(e), the TEM image of Cu_4/CF clearly indicated that CeO_2 crystal could be easily identified while very little Fe_2O_3 phase was found. The amorphous Fe_2O_3 may be dispersed among the CeO_2 crystal and/or incorporated into CeO_2 lattice.

It's expected that XRD peaks of Fe_2O_3 are shaded by the strong peaks of CeO_2 when both Fe_2O_3 and CeO_2 phases are present. In order to qualitatively compare the amount of Fe_2O_3 and CeO_2 crystals, the intensity ratios of IFe ((104) plane of Fe_2O_3 at 33.1°) and ICe ((111) plane of CeO_2 at 28.6°) are calculated with the results (IFe/ICe) listed in the inserted tables of Fig. 4(a). It should be noted that although the peaks at 28.6° are also contributed by CeO_2, the ratio of IFe/ICe could represent the relative intensities of Fe_2O_3 and CeO_2 diffraction. Ce/CeO_2 shows the smallest IFe/ICe ratio since Fe_2O_3 phase is not included and the peak IFe is only contributed by (200) plane of CeO_2. Sample MM show bigger IFe/ICe ratio due to the contribution of Cu/Fe_2O_3. The samples with CF supports, no matter loaded with copper or not, exhibit the highest IFe/ICe ratios than samples of other oxide support. Fe_2O_3 crystals give stronger diffraction intensities when co-synthesised with CeO_2. It is speculated that Fe_2O_3 phase are mainly formed on the surface of CeO_2 lattice in the CF involved samples, and these 'topped' Fe_2O_3 phase could be more easily detected by XRD comparing to the mixed Fe_2O_3 crystals in sample MM. The 'topping' of Fe_2O_3 phase on

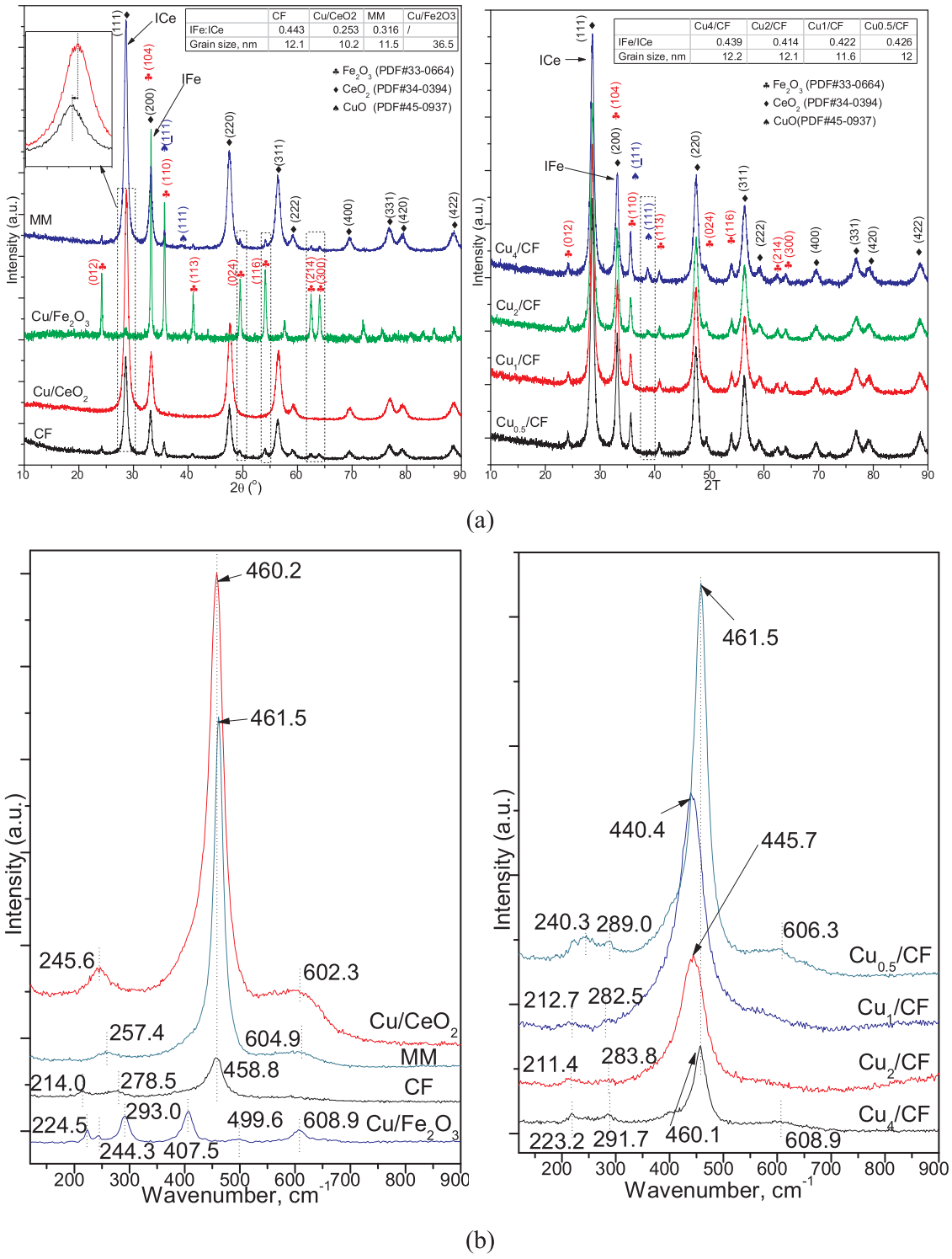

Fig. 4. The XRD pattern (a) and Raman spectra (b) of prepared catalysts. (Note: ICe:IFe is the intensity ratio of peaks IFe and Ice. By Debye-Scherrer Equation, the grain sizes of CeO_2 are calculated for CF, Cu/CeO_2 and Cu_x/CF, and grain size of Fe_2O_3 is calculated for Cu/Fe_2O_3.).

the CeO_2 crystals may also facilitate the incorporation of iron atoms into CeO_2 lattice. Other peaks of Fe_2O_3 also exhibit stronger intensities on the CF involved samples than those on sample MM. The gain sizes of the samples are further calculated by Debye-Scherrer Equation with the results listed in the inserted tables of Fig. 4(a). The grain size of Cu/CeO_2 is 10.2 nm. When iron is co-synthesised into the support, the grain sizes of most CF involved samples are over 12 nm. It's again speculated that topping of Fe_2O_3 could significantly increase the grain size.

Raman spectroscopy, a potential tool and sensitive to metal-oxygen arrangement and lattice defects, was performed to obtain additional structural information. The Raman spectra of different catalysts are shown in Fig. 4(b). Over catalyst Cu/Fe_2O_3, peaks at bands at 224.5, 244.3, 407.5, 499.6, and 608.9 cm^{-1} could be ascribe to hematite α-Fe_2O_3 [39–41]. For sample Cu/CeO_2, the Raman spectra present a characteristic peak at around 460 cm^{-1}, corresponding to the F_{2g} vibration mode of octahedral local symmetry around cubic fluorite structure of CeO_2 [42–44]. The broad shoulder at 602 cm^{-1} and a weak band at 246 cm^{-1} could be attributed to the oxygen vacancies

[23,42,44]. The Raman spectra could well confirm the conclusions made from XRD patterns that the main supports of Cu/CeO_2 and Cu/Fe_2O_3 are hematite α-Fe_2O_3 and fluorite CeO_2, respectively. When catalysts Cu/CeO_2 and Cu/Fe_2O_3 are mixed, peaks of Fe_2O_3 are shaded and become invisible. The main peak and oxygen defects caused shoulders could also be detected at similar positions.

When ion oxides and copper oxides are synthesized together, the main band at around 460 cm^{-1} become much smaller over sample CF, which could be explained by the topping of Fe_2O_3 phase over CeO_2 lattice, as discussed in the XRD part. All the supported copper catalysts Cu_x/CF show similar Raman spectra pattern with the CF support, exhibiting clear evidence of CeO_2 crystals. The structure of CeO_2 lattice is very important for characteristics of these catalysts. Comparing with Cu/CeO_2 catalyst and the solid mix, the bands at ~460 cm^{-1} of most CF catalysts redshift to lower wavenumber, which could be caused by the incorporation of Fe and/or copper into CeO_2 lattice [23]. The ruffles in 211–290 cm^{-1} could be contributed by the presence of Fe_2O_3, which is not present in sample Cu/CeO_2. More ruffles could be observed over the CF supporting catalyst, comparing to samples Cu/CeO_2 and MM. It is indicated that Fe_2O_3 phase are more visible over CF involved samples, which is in line with observation of XRD. The Raman lines of CuO are absent in all of the samples, indicating that the copper oxide species are in the forms of highly dispersed and clustered states.

3.3. Chemical properties (XPS, H_2-TPR, and EPR)

3.3.1. XPS

XPS spectra of the samples Cu_4/CF, Cu/CeO_2 and Cu/Fe_2O_3 were taken to investigate the chemical valence state of main components with the results shown in Fig. 5. Fe 2p spectra of samples Cu_4/CF and Cu/Fe_2O_3 are presented in Fig. 5(a). For catalyst Cu/Fe_2O_3, peak positions of Fe $2p_{1/2}$ at 725 eV, Fe $2p_{3/2}$ at 711.5 eV, and satellite at 719 eV are in accordance with the characteristics of Fe^{3+} in Fe_2O_3 [45], indicating that the formed oxides are mainly Fe_2O_3. When ion is synthesised together with CeO_2, the Fe 2p peaks are broader and lower, and the positions are quite different over catalyst Cu_4/CF, significantly shifting to higher binding energies, with Fe $2p_{1/2}$ at 734 eV and Fe $2p_{3/2}$ at 718 eV. It is quite clear that the synthesised ion oxides are quite different with bare Fe_2O_3 phase. The interaction of Ce strongly changed with chemical state of Fe. To our knowledge, there is no report for the ion oxides with Fe 2p peaks with such high binding energies. The broad Fe 2p peaks may consist of incorporated Fe, dispersed Fe and clustered Fe oxides. It is speculated certain amount of ion atoms are incorporated into the CeO_2 lattice and the interaction of Ce and O atoms with Fe atoms in the CeO_2 lattice could result in the significant shifting of observed binding energies. At the same time, dispersed and clustered Fe could also interact with CeO_2 lattice and result in the change of chemical properties. The intensities of Fe 2p peaks are weaker than those on Cu/Fe_2O_3 catalyst and may be interpreted to be caused by the high dispersion of ion oxides over CeO_2 crystals as indicated by TEM results.

The XPS spectra of Ce 3d over samples Cu_4/CF and Cu/CeO_2 are shown in Fig. 5(b). The XPS spectra of Ce 3d over these two samples are almost identical, typical of Ce^{4+} and a small quantity of Ce^{3+} [23]. Thus the chemical state of Ce species is not changed whether Fe is synthesised together. Combining the observations of TEM, XRD and Raman spectra, it could be further confirmed the same CeO_2 lattice was formed in these catalysts. The presence of massive Fe didn't affect the main structure of CeO_2 lattice. By comparison, the chemical state of Fe is altered by CeO_2 lattice, but the state of Ce is not influence by Fe, implying that Fe is incorporated into the CeO_2 lattice instead of the incorporation of Ce into Fe_2O_3 lattice. It now well explains why only CeO_2 cubic phase could be observed in the TEM image and why CeO_2

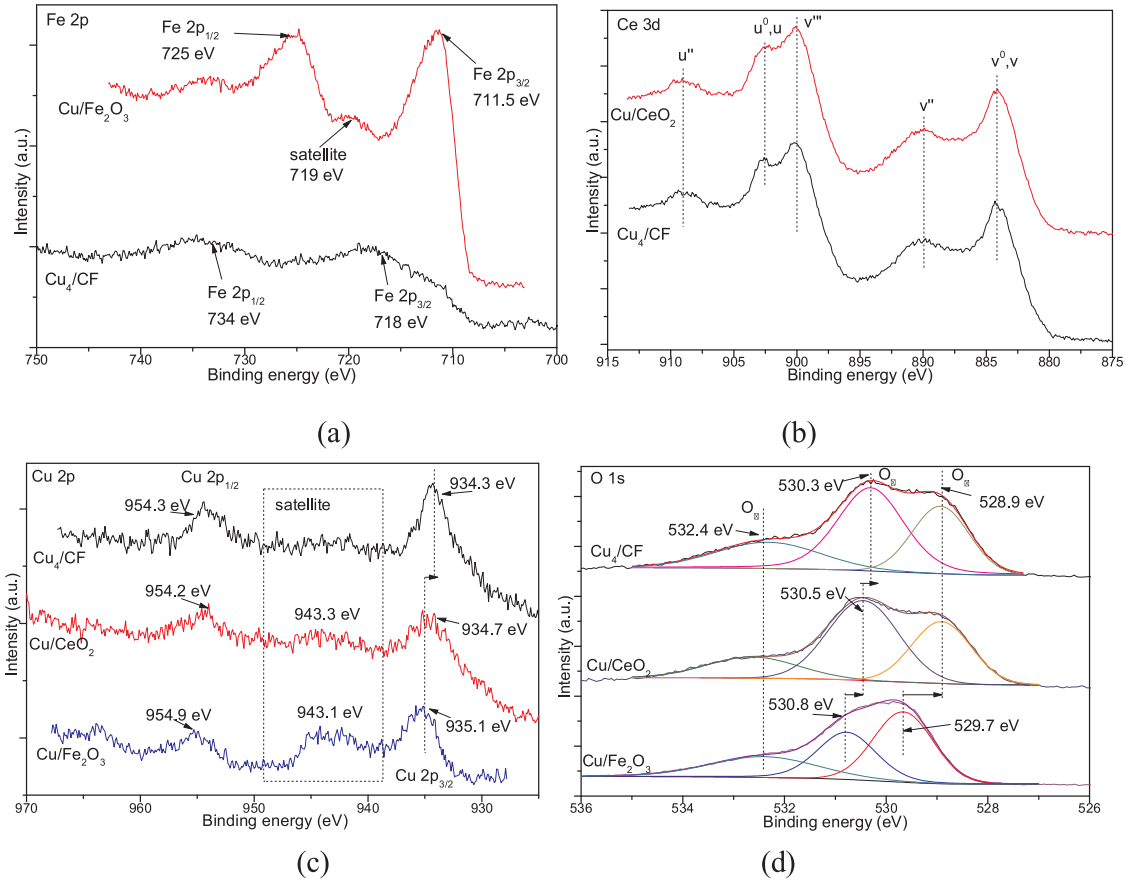

Fig. 5. XPS spectra. (a) Fe 2p; (b) Ce; (c) Cu 2p; (d) O 1 s.

Table 2
Composition of oxygen species calculated by XPS spectra.

Component	Cu_4/CF	Cu/CeO_2	Cu/Fe_2O_3
Lattice O_α (%)	29.95	32.73	43.70
Vacancy O_β (%)	48.11	50.14	31.31
Surface O_γ (%)	21.94	17.12	24.99

crystals show much stronger XRD and Raman intensities.

For Cu 2p over all three catalyst samples in Fig. 5(c), peaks of Cu $2p_{1/2}$ at 954.2–954.9 eV and Cu $2p_{3/2}$ at 934.3–935.1 eV are typical of Cu^{2+} [23]. The satellite at around 943 eV is also featured for Cu^{2+}. Thus the impregnated copper species are mainly Cu^{2+} in CuO. It should be noted that peak of Cu $2p_{3/2}$ on sample Cu_4/CF slightly shift to lower binding energy comparing to those over samples Cu/CeO_2 and Cu/Fe_2O_3. The satellite also disappears. It's implied that mixed oxide support CF could facilitate the formation of Cu species with lower chemical valence, which may further enhance the catalytic redox reaction.

Concerning oxygen in the catalyst samples, XPS spectra in Fig. 5(d) could be deconvoluted into three peaks and ascribed to lattice oxygen O_α at 528.9 eV (lattice oxygen bound to metal cations), vacancy oxygen O_β at 530.3 eV (oxygen in the lattice as M-O-M which may later be vacated as M-□-M during catalytic reactions), and surface oxygen O_γ at 532.4 eV (surface oxygen, such as oxygen contamination, $-OH$, $-CO_3$ and absorbed O_2), respectively [13,42]. The fractions of each oxygen species could be calculated according to the area ratios of these peaks and are summarized in Table 2. Cu/Fe_2O_3 presents less O_β and more O_α than Cu_4/CF and Cu/CeO_2. It has been frequently considered that O_β is essential for the catalytic activity since vacancy oxygen plays a key role in the oxygen transfer during the redox reaction [13,42]. This explains the poorer catalytic performance of Cu/Fe_2O_3. The fraction of O_β and O_α are similar on samples Cu_4/CF and Cu/CeO_2, confirming the similar lattice structure of CeO_2 and CF supports. It should be noted that the existence of large amount of Fe_2O_3 (which has less O_β than Cu/CeO_2) in catalyst Cu_4/CF could dilute O_β, resulting in a lower fraction of O_β. But the value of O_β fraction in catalyst Cu_4/CF is similar with that of Cu/CeO_2, implying that oxygen vacancy in CeO_2 lattice is increased by Fe doping. The positions of oxygen species follow an order of Cu_4/CF < Cu/CeO_2 < Cu/Fe_2O_3 (binding energy). Lower binding energies of oxygen on Cu_4/CF and Cu/CeO_2 may also facilitate the redox cycle of oxygen during catalytic reactions.

3.3.2. H_2-TPR

H_2-TPR was then tested for the reducibility properties of catalysts and the results are presented in Fig. 6. In Fig. 6(a), purchased pure CuO sample was tested as a reference. Peak of CuO was found to be at 377 °C. When copper is loaded onto the CeO_2 support, the CuO peak on Cu/CeO_2 sample shifts to 265 °C with a shoulder at 209 °C. The dispersion of CuO over oxide support could greatly enhance its reducibility as widely recognized in literature [38]. The minor peak at 433 °C could be ascribed to small amount of amorphous surface CeO_2 while peak at 829 °C is attributed to large bulk CeO_2 crystals [28,46].When impregnated onto Fe_2O_3 (sample Cu/Fe_2O_3), peak of copper shows up at 211 °C. The broad peak at 650 °C is attributed clustered Fe_2O_3 (aggregated big Fe_2O_3 clusters), including the three step reduction $Fe_2O_3 \rightarrow Fe_3O_4 \rightarrow FeO \rightarrow Fe$ [47]. Peak at 313 °C could be attributed to the dispersed ion oxides (fine Fe_2O_3 crystals). The TPR profile of sample CF also exhibits peaks at 601 °C and 335 °C of clustered Fe_2O_3 and dispersed ion oxides (these dispersed Fe_2O_3 could also be the topped Fe_2O_3 phase on CeO_2 lattice surface), confirming the interpretation of Cu/Fe_2O_3 profile where peak at 211 °C, instead of that at 313 °C, was assigned to copper oxides. Peak of CeO_2 could also be observed at 801 °C. When Cu/Fe_2O_3 and Cu/CeO_2 were mixed (sample MM), peaks of all the involved oxides could be observed in the H_2-TPR profile, with CuO at 202 °C, dispersed Fe_2O_3 at 308 °C, clustered Fe_2O_3 at 638 °C, and CeO_2 at 857 °C.

When copper is impregnated onto the co-synthesized support CF (sample Cu_4/CF in Fig. 6(b)), similar peaks could be observed for these oxides. But it should be noted that peak of copper shifts to a lower temperature, 179 °C. Peak of dispersed Fe also decreases significantly, comparing to sample solid mix. It could be explained that more dispersed Fe could be incorporated into the CeO_2 lattice (incorporated Fe), resulting in a weaker peak intensity. This Fe peak also shifts slightly to higher temperature. It may be caused by the interaction of dispersed Fe and CeO_2 lattice since Fe incorporated into CeO_2 lattice may become more difficult to be reduced. In contrast, the peak for CeO_2 at higher temperatures moves to lower temperature, from 857 °C in sample MM to 800 °C in Cu_4/CF, which could be explained by the lattice deformation due to Fe incorporation. Although XRD, Raman and TEM results indicated that the main crystals over Cu/CF samples are CeO_2 lattice, H_2-TPR profiles show a dramatically different reducibility of CF lattice with CeO_2 lattice. The interaction of Fe and Ce is expected to be very important for the chemical property of the catalyst than the observed physical structure.

Here we further calculated the amount of Fe incorporated into the CeO_2 lattice. There are three types of Fe in the catalyst samples, incorporated Fe', dispersed Fe" (with TPR peak at 300–340 °C), and clustered Fe"' (with TPR peak at 570–640 °C). The amount of Fe" and Fe"' could be directly calculated from the area of corresponding TPR peaks. When incorporated into the CeO_2 lattice, Fe' is expected to exhibit higher reduction temperature than Fe" and Fe"'. Thus Fe' in the CeO_2 lattice is assumed to have similar reduction temperature as CeO_2 and the TPR peak could be merged with the CeO_2 peaks at above 800 °C. The amount of Fe' could then be obtained from the total amount of Fe (theoretical amount calculated from the loaded Fe) and the calculated values of Fe" and Fe"' by: [Fe'] = [Theoretical]-[Fe"]-[Fe"']. Table 3 summarizes the calculation results of different Fe species over different catalyst samples. Over sample MM, Fe is not incorporated into the CeO_2 lattice. The total amount of Fe' and Fe" is higher than the theoretical value due to H_2 spill over effect [38]. Over samples CF and Cu_4/CF, the fractions of Fe' are calculated to be 9.84% and 8.54%, respectively. The fractions of dispersed Fe" are lower than that over sample MM, since significant amount of dispersed Fe", which contacts closely with CeO_2 lattice, could be incorporated into the lattice and become Fe'.

The reduction temperatures of CuO and CeO_2 over sample Cu_4/CF are lower than that of pure CuO and Cu/CeO_2. It follows that the interaction of Cu oxide with CF support favourably promotes the reduction of Cu oxide and diffusion of surface oxygen species at low temperatures. Consequently, the electronic property and structural environments of Cu^{2+} ions were greatly changed compared to that of bulk CuO [42].

The shifting of peak positions to lower temperature region at higher copper loading has been frequently reported in literature [13,30,38]. Typical interpretation is that peaks at around 150 °C and 180 °C are the stepwise reduction of dispersed CuO. Peak at above 220 °C represents crystalline CuO, which increase accordingly with copper loading [30,38]. In our study, peak at 150 °C is not always present and peak at above 220 °C doesn't increase with copper loading. Thus this interpretation is not applicable. Someone explained the peak shifting by hydrogen spill over effect [38]. Others explained that the peak at around 150 °C is associated with reduction of surface dispersed Cu oxide that weakly interacts with the support, while peaks appearing between 200–250 °C are associated with reduction of the surface dispersed Cu species that strongly interacts with the support [13].

In this study, we ascribe Cu' to dispersed CuO that strongly interact with CF support, where stronger interaction of CuO and CF lattice makes it difficult to be reduced and result in a high reduction temperature. Cu" is the dispersed CuO that weakly interact with CF support, which is considered to be mainly single layer CuO. Cu"' is attributed to the CuO dispersed over other CuO oxides, which are double

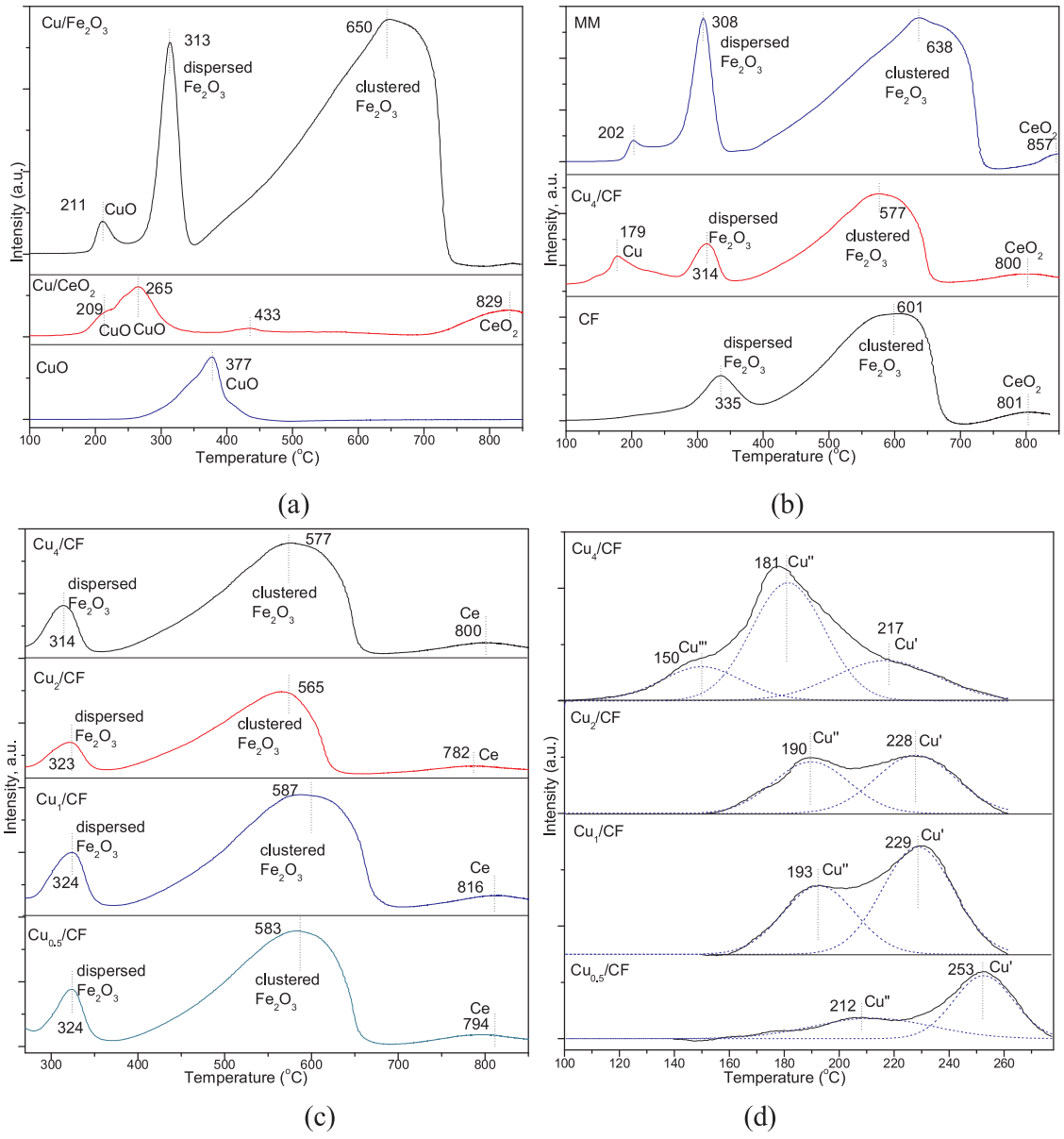

Fig. 6. H_2-TPR profiles. (a) CuO, Cu/CeO_2 and Cu/Fe_2O_3; (b) CF, Cu_4/CF and MM; (c) Cu_x/CF at 280–850 °C; (d) Cu_x/CF at.100–280 °C.

or multi layer CuO, where extremely weak interaction between these CuO and CF support makes these oxides easy to be reduced and is represented by the low reduction temperature. At lower copper loading, most of the dispersed CuO (Cu') could directly contact with CF support and strongly interact with the CF lattice. With the increased loading of copper, the amount of CuO (Cu") that weakly interacts with the CF support increases accordingly. If copper loading is further increased, double or multi layer CuO (Cu'") appears. At the same time, the amount of Cu' does not increase significantly with copper loading, as indicated in Table 4, since the CF lattice that could strongly interact with or incorporate CuO may be saturated. Clustered CuO may appear at above 300 °C and could be shaded by the peaks of dispersed Fe_2O_3. The existence of the shaded clustered CuO could be confirmed by the total amount of H_2 consumption, which is lower than the theoretical values

Table 3
H_2-TPR calculation of different Fe species.

Sample	Peak position (°C)			H_2 consumption (μmol/g cat)				Fraction of Fe species %		
	Fe' [a]	Fe"	Fe"'	Fe' [b]	Fe"	Fe"'	Theoretical[c]	Fe'	Fe"	Fe"'
MM	/	308	638	/	911.9	5809.9	5654.8	/	13.57	86.43
CF	> 800	335	601	508.3	460.2	4638.2	5952.4	9.84	8.14	82.02
Cu_4/CF	> 800	314	577	556.3	460.2	4638.2	5654.8	8.54	8.99	82.47

Note: a), TPR peak of Fe' is assumed to be merged with CeO_2 peak at above 800 °C.
b), H_2 consumption of Fe': [Fe'] = [Theoretical]-[Fe"]-[Fe"'].
c), Theoretical H_2 consumption calculated from the amount of Fe in the samples.

Table 4
H_2-TPR calculation of different Cu species.

	Peak position (°C)			H_2 consumption (μmol/g cat)					
	Cu'''	Cu''	Cu'	Cu'''	Cu''	Cu'	Cu' + Cu''	Total	Theoretical*
$Cu_{0.5}$/CF	/	212	253	/	44.3	68.1	112.4	112.4	53
Cu_1/CF	/	193	229	/	79.3	122.7	202	202.0	87
Cu_2/CF	/	190	228	/	101.6	119.2	220.8	220.8	172
Cu_4/CF	150	181	217	49.8	153.0	73.1	226.1	276.1	355

* Based on Cu loading determined by ICP in Table 1.

at higher copper loading (Cu_2/CF and Cu_4/CF). The higher H_2 consumption than the theoretical values at lower copper loading could be caused by H_2 spill over effect.

At lower Cu loading, the interaction of CuO with CeO_2 lattice is stronger, making the reduction of CuO more difficult. At higher Cu loading, the interaction is weaker, making the reduction of CuO easier. However, the catalytic NO + CO reaction is more significantly influenced by the synergetic effects of CuO and CF support. Thus although CuO is more easily reduced at higher copper loading, the catalytic activity for NO + CO reaction, mainly in terms of TOF as shown in Fig. 1(f), does not necessarily increase at the same time. On the other hand, the increased reducibility of CF support at 577 °C for clustered Fe_2O_3 and at 800 °C for CeO_2 lattice comparing to other supports, may also contribute to its excellent catalytic performance.

NO conversions were further normalized by the amount of Cu' + Cu'' and plotted in Fig. 1(g) to explore the relationship between catalytic activity and copper-support interaction. It could be observed that most values of normalized NO conversions are similar at each temperature. Two exceptions could be observed over sample $Cu_{0.5}$/CF at 200 °C and 250 °C. The much higher values of these two data could be explained by the similar NO conversions (about 100%) at high temperatures over all samples but much lower copper loading over $Cu_{0.5}$/cf. For comparison, NO conversions were also normalized by individual Cu' and Cu'', respectively, with the results provided in the supplementary information (Figs. S4 (a) and (b)). The big variations of normalized NO conversions at each temperature suggest that NO reduction does not depend on individual Cu' or Cu''. On the contrary, the close values of most normalized NO conversions by Cu' + Cu'' imply that Cu' and Cu'' together determines the catalytic activities. The dispersed copper species, both strongly and weakly interacting with CF support, are active for NO + CO reaction. The multi-layer Cu''', which does not directly contact with CF support, doesn't contribute to NO reduction. In the catalytic activity section, it was observed that aggregated copper clusters at high metal loadings could decrease both NO conversion and N_2 selectivity. This could be explained that the aggregated copper, which is obviously Cu''', has little contribution to NO reduction, but inhibits the contact of NO and CO with Cu' and Cu'', resulting in a worse catalytic performance.

3.3.3. EPR

The state and coordination environment are further analyzed by EPR spectra as shown in Fig. 7. For Cu/Fe_2O_3 sample, no obvious ERP signal could be identified since Fe^{3+} doesn't show EPR lines and copper is highly dispersed over the catalyst at low loadings. For Cu/CeO_2 sample, the signal characterized by a broad signal (line width = 160 G) centered at g_{av} = 2.11 is attributed to dipolar, interacting Cu^{2+} ions forming a nano-sized 2-dimensional structure [48]. The strong resonance line at $g_{\parallel}$ = 2.033 and $g_{\perp}$ = 2.009 is attributed to O_2^- species bound to Ce^{4+} ions [31,48]. The additional signal at g = 2.044 is due to the presence of Ce^{3+} ions and oxygen vacancies [31]. The ERP profile of sample MM is similar with that of Cu/CeO_2, indicating that the mechanically mixed Fe_2O_3 supported samples doesn't change the coordination environment of the support. After doping Fe into the CeO_2 support (sample CF), the EPR profiles change significantly, implying the incorporation of Fe into the CeO_2 lattice could modify the coordination environment of the support, which was not so clearly indicated by the physical characterizations, such as TEM and XRD. Two additional signals appear, one at g = 2.025 ascribed to paramagnetic O_2^- species resulting from the oxygen vacancy [13], and one at g = 1.95 assigned to Ce^{3+} ions [31,48]. The appearance of these additional signals indicates the more strongly unsaturated coordination environment of the surface CeO_2 support after Fe doping. For Cu/CF samples, the positions of observed EPR signals are similar with those of CF support. The broad signal of Cu^{2+} become less visible due to the interaction of Cu with CF supports. There is strong dependence of the spectra structure and parameters on the copper loading. The intensities of all the CF lattice related peaks decrease with the increased copper loading since CF lattice is shaded by the topping of dispersed CuO.

3.4. Possible framework of Cu/CF

Based on physical and chemical characterization, it could be concluded that the main framework of CF support is CeO_2 lattice and certain amount of iron could be incorporated into the CeO_2 lattice. The structure of the modified support lattice and synergistic effect between CF support and copper are essential for the catalytic activity. The oxygen vacancy in CeO_2 lattice is caused by the replacement of Ce^{3+} into Ce^{4+} positions, as expressed tentatively in Eq. (1) [43]. Similarly, when Ce^{4+} in the lattice is replaced by lower state ion Fe^{3+}, one oxygen in the lattice is ejected to keep the valance balance, producing one oxygen vacancy in the lattice, as expressed in Eq. (2) [43] and Fig. 8(a). The incorporation of Fe into CeO_2 lattice could generate a significant amount of oxygen vacancy, which could further become the active reaction sites on the catalyst.

$$Ce_2O_3 \xrightarrow{2CeO_2} 2Ce'_{Ce} + 3O_O + V''_O \quad (1)$$

$$Fe_2O_3 \xrightarrow{2CeO_2} 2Fe'_{Ce} + 3O_O + V''_O \quad (2)$$

The structure of the Cu_x/CF catalyst is then proposed in Fig. 8(b). The main framework of the support is CeO_2, as shown in Fig. 8(b, left). The co-synthesised iron could be incorporated into the CeO_2 lattice, as indicated in Fig. 8(b, middle). Copper that strongly interact with the CF support is expected to play a key role in the redox reaction. The structure of copper interacting with CF is illustrated in Fig. 8(b, right).

3.5. H_2O and SO_2 resistance

H_2O and SO_2 resistance is of great significance for catalysts since the presence of H_2O and SO_2 are inevitable in the flue gas. The catalytic performance was tested with the presence of H_2O and/or SO_2 and the results are shown in Fig. 9. For catalyst Cu_4/CF, the effect of H_2O is minor on the NO reduction efficiency with NO_x conversion decreasing slightly from 99.5% to 96% at 200 °C when H_2O is added into the modeled flue gas. Then when H_2O is removed, NO_x conversion efficiency recovers to 96.5%. When SO_2 is added, NO_x conversion decreases rapidly from 99.5% to 92% in 10 min. It then slowly decreases to 88.6% in 60 min as the catalyst is constantly deactivated by SO_2. After SO_2 is removed, NO_x conversion recovers to 91.5%. When both SO_2 and H_2O are added, NO_x conversion decreases rapidly from 99.5%

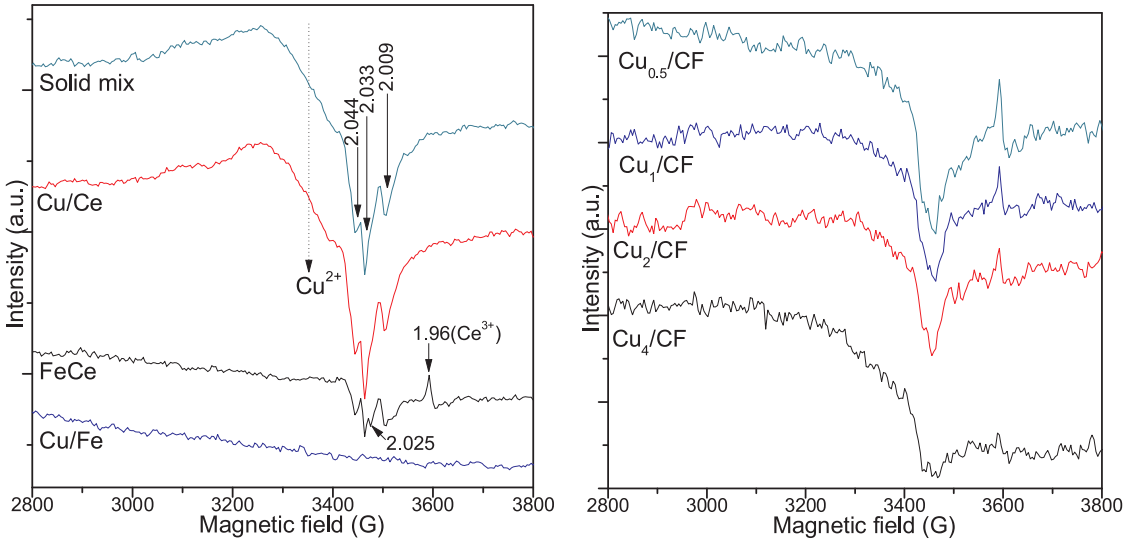

Fig. 7. EPR spectra.

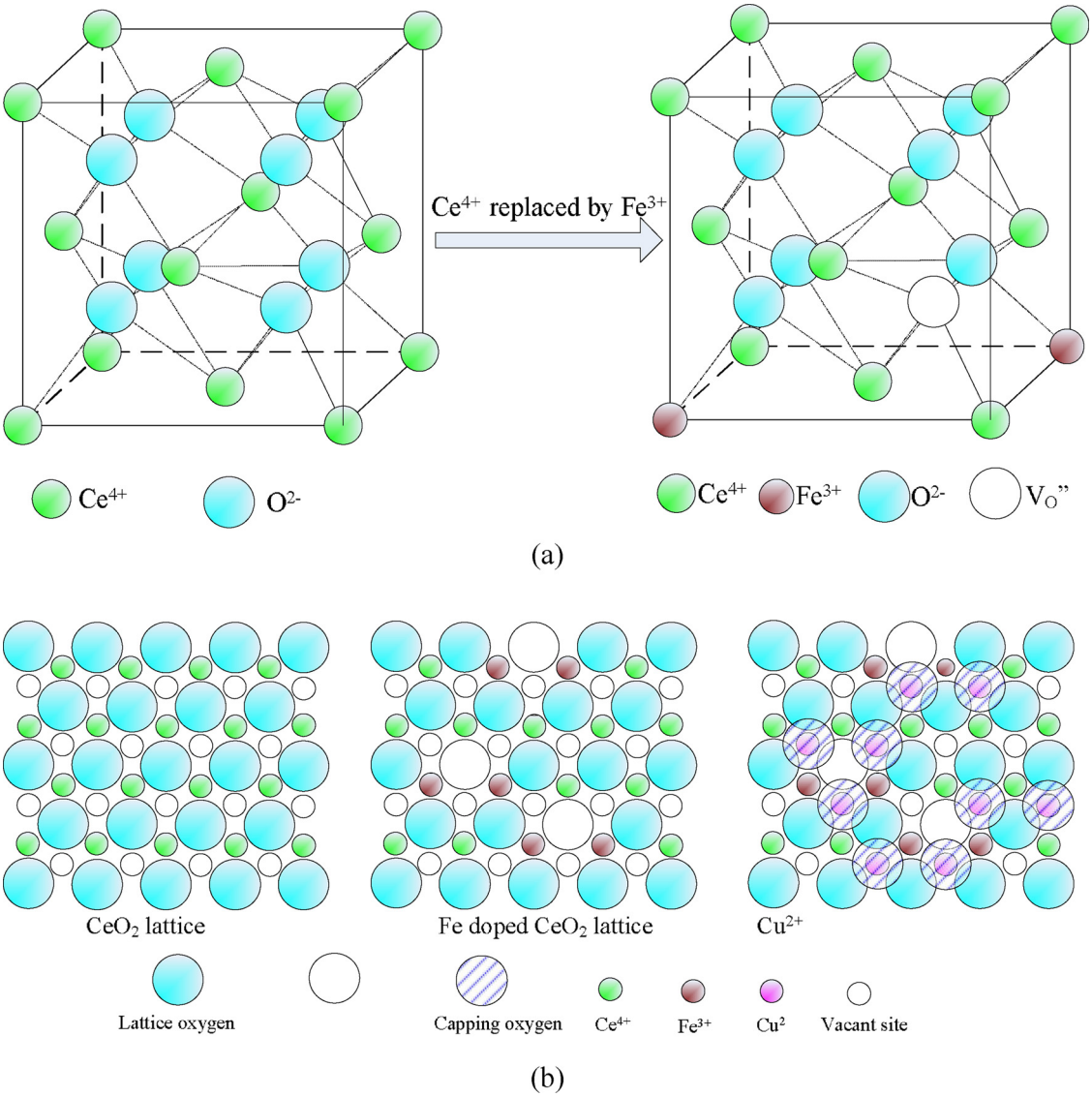

Fig. 8. Possible framework of Cu/cf. (a), variation of unit cell of CeO_2 during Fe doping process; (b) Diagram of Cu^{2+} incorporated in the vacant sites on the (111) plane of the CF supports.

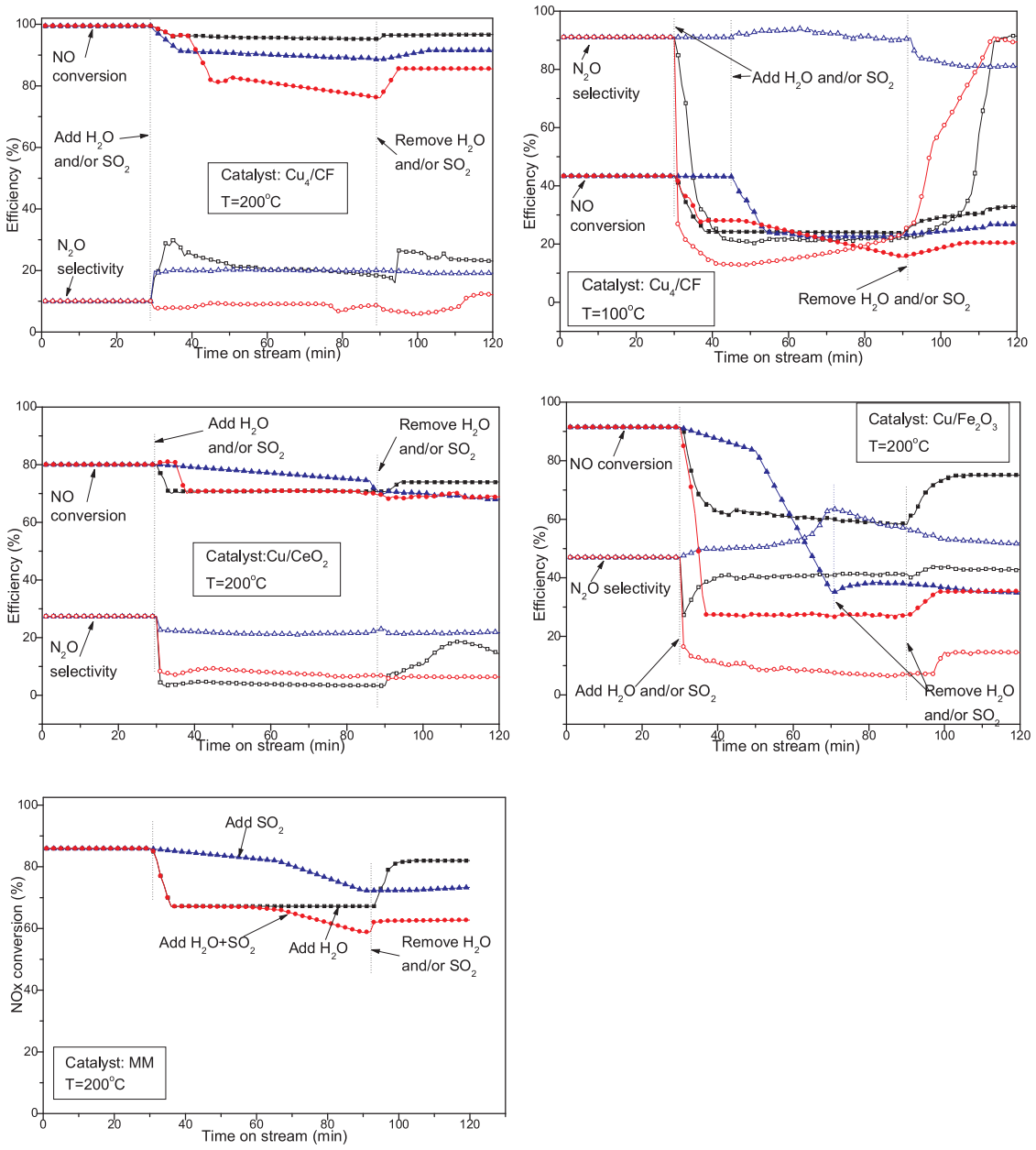

Fig. 9. Influence of H_2O and/or SO_2 on the catalytic performance. (Reaction condition: initial NO = 800 ppm, NO:CO = 1:2, H_2O = 10%, SO_2 = 100 ppm, GHSV = 30,000 h^{-1}). (Symbols: solid, NO conversion; open, N_2O selectivity. Black: add/remove H_2O, blue: add/remove SO_2, red: add/remove H_2O + SO_2.) (For interpretation of the references to colour in this figure legend, the reader is referred to the web version of this article).

to 81.5% in 20 min. Then the decreasing is slowed down as NO_x conversion decreases to 76% in 40 min. After SO_2 and H_2O are removed, NO conversion recovers to 85.5%. The irreversible deactivation of the catalyst could be caused by the formation of stable sulphates which could not be decomposed by CO. The presence of both H_2O and SO_2 could promote the formation of H_2SO_4 and then enhance the production of the stable sulphates, $CuSO_4$, leading to the rapid loss of active metal sites. The deactivated catalysts could be hardly recovered even after regenerated in air at 500 °C as shown in the supplementary information (section S4). At lower temperatures, the effect of H_2O and SO_2 is more serious. At 100 °C, when H_2O, SO_2, and SO_2+H_2O are added, NO conversions rapidly decrease from 43.3% to 24.3%, 24.5%, and 28%, respectively. When H_2O, SO_2, and H_2O + SO_2 are removed, NO conversions only recover to 32.8%, 26.8%, and 20.4%, respectively. Overall speaking, Cu_4/CF catalyst exhibits good H_2O resistance at high temperatures (200 °C) due to its excellent catalytic performance. The SO_2 resistance is also acceptable with 15% irreversible deactivation in about 1 h. Both reversible and irreversible deactivations are faster when H_2O and SO_2 are presented together in the flue gas. The H_2O and SO_2 resistance is much poorer at lower temperatures (100 °C) and the irreversible deactivation is much more serious. The higher adsorption rate of H_2O and SO_2 at lower temperatures may hinder the contact of active sites and NO_x species and further contribute to the poor resistance.

For catalyst Cu/Fe_2O_3, H_2O and SO_2 resistances are very poor. At 200 °C, NO_x conversions decrease significantly from 91.4% to 62%, 35%, and 27%, respectively, when H_2O, SO_2, and H_2O + SO_2 are added. After H_2O is removed, NO_x conversion recovers to 75%. But the recoveries are minor when SO_2 and SO_2+H_2O are removed, indicating the serious and irreversible deactivating effect of SO_2 and H_2O. Catalyst Cu/CeO_2 exhibits better H_2O and SO_2 resistance than catalyst Cu/Fe_2O_3 at 200 °C. NO_x conversions decreased from 80% to 70.7%, 74.5%, and 70%, respectively, when H_2O, SO_2, and H_2O + SO_2 are added. But the

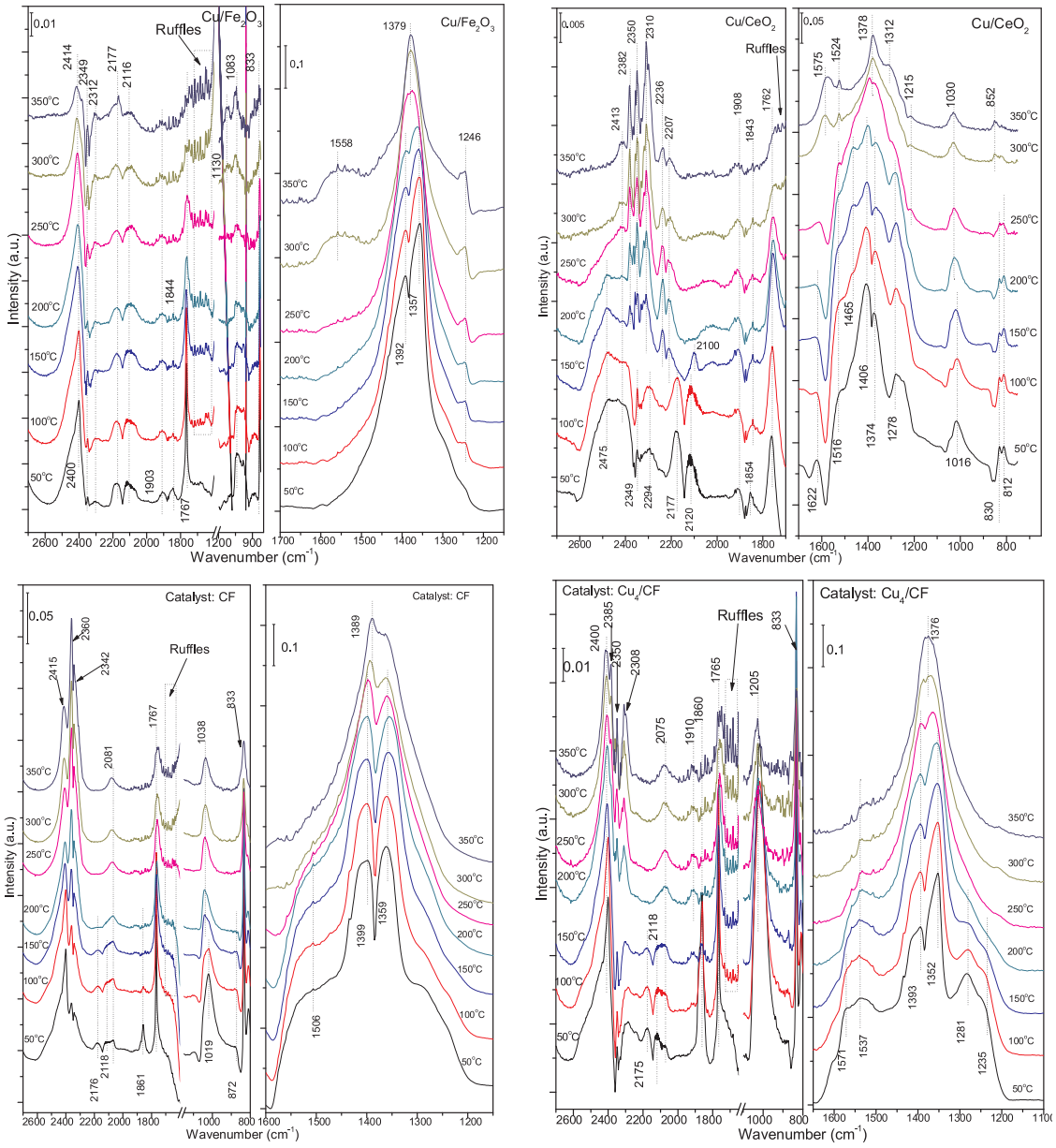

Fig. 10. *in situ* DRIFT spectra of NO + CO reaction. (Reaction condition: NO = 5000 ppm, CO = 5000 ppm, balanced with Ar).

catalytic activities are not recovered when SO_2 and $H_2O + SO_2$ are removed. The resistance of SO_2 and/or H_2O over solid mix is between the performance of Cu/Fe_2O_3 and Cu/CeO_2.

By comparing the performances of the four catalysts, it could be concluded that the performance of Cu_4/CF for H_2O and SO_2 resistance is similar with catalyst Cu/CeO_2 and is much better than catalyst Cu/Fe_2O_3. CeO_2 supported catalysts shows better H_2O and SO_2 resistance than Fe_2O_3 supported catalysts. Since the inhibition effect of H_2O is generally considered to be due to the competitive chemisorption of H_2O [20,36,49], it is speculated that faster H_2O chemisorption over Fe_2O_3 may the reason of its poor water resistance. The easier formation of Fe_2SO_4/Fe_2SO_3 may lead to the poor SO_2 resistance. Comparing the performance of Cu_4/CF and sample MM, it could be observed that the SO_2 resistance is poor no matter Fe is mechanically mixed with CeO_2 supported catalyst or doped into CeO_2 lattice, confirming the speculation of Fe_2SO_4/Fe_2SO_3 formation. The H_2O resistance of Cu_4/CF is much better than sample MM, indicating that the Fe doped CeO_2 lattice could retain (or show even better) good water resistance of CeO_2 supported catalysts but mechanically mixed samples can't. The interaction of Fe and CeO_2 lattice could enhance both catalytic performance and water resistance.

Concentrations of N_2O at the outlet were also measured with N_2O selectivity calculated and presented in Fig. 9 together with the NO conversions. When SO_2 is added, N_2O selectivity increases for most cases, indicating that the deactivation by SO_2 could inhibit the reduction of NO into N_2 and increase the production of undesired N_2O. However, N_2O selectivity decreases when H_2O and $H_2O + SO_2$ are added, although the addition these components could inevitably suppress NO conversions. One should note that the decrease of N_2O selectivity does not necessarily mean the increase of N_2 formation because other reaction intermediates instead of N_2O could be produced when H_2O is present. We observed the existence of certain amount of NH_3 in these cases, which could be formed by water-induced hydroxylation promoting NH_3 formation [50].

3.6. *In situ* DRIFT study and reaction mechanism

In order to further explore the reaction mechanism, *in situ* DRIFT

Table 5
Summary of DRIFT spectra.

Wavenumber (cm^{-1})	Assignment and reference	Catalyst sample	Evolution behaviour (as temperature increased)
2400–2415	NO^+ [51]	Cu/Fe_2O_3, CF, Cu_4/CF	Decrease
		Cu/CeO_2;	Decrease very fast
2382–2385	CO_2	Cu/CeO_2; Cu_4/CF	Increase
2360, 2342	CO_2, P and R branch	CF	Increase
2349–2350, 2308–2312	CO_2	Cu/Fe_2O_3, Cu_4/CF	Increase
		Cu/CeO_2	Increase with high intensity
2236, 2207	N_2O [24]	Cu/CeO_2	Appear at 150 °C, first increase, then decrease slowly at above 200 °C
2175–2177	Cu^+-CO [42]	Cu/Fe_2O_3	Decrease slowly
		Cu/CeO_2	Decrease, disappear at above 100 °C
		CF, Cu_4/CF	Decrease, disappear at above 150 °C
2116–2120	Physical adsorbed CO [42]	Cu/Fe_2O_3	Decrease slowly
		$CuCeO_2$, CF, Cu_4/CF	Decrease, disappear at above 150 °C
2100	Cu^+-CO [13,23]	$CuCeO_2$	Appear at 150 °C
2081	Cu^+-CO [13,23]	CF	Increase
1903–1910	Cu^{2+}-NO [51]	Cu/Fe_2O_3	Decrease
		Cu/CeO_2	First increase, then decrease
		Cu_4/CF	Increase
1860–1861	Physical adsorbed NO [51]	CF, Cu_4/CF	Decrease fast at below 150 °C, become broad noise-shape ruffles at above 150 °C
1843–1844	Cis-$(NO)_2$, v_s(N-O) [51]	Cu/Fe_2O_3	Decrease fast, become broad noise-shape ruffles at above 150 °C
		Cu/CeO_2	Decrease slowly
1762–1767	Trans-$(NO)_2$, v_{as}(N-O) [51]	All	Decrease fast, sharp peak becomes lower and broader
Ruffles between 1720–1625	NONO [51]	Cu/Fe_2O_3, CF, Cu_4/CF	Increase fast
		Cu/CeO_2	Appear at above 300 °C
1392–1399, 1357–1359	M-NO_2 [51]	Cu/Fe_2O_3, Cu_4/CF	Decrease, disappear at above 250 °C
		CF	Decrease, could be observed even at 350 °C
1379	Free NO_3^- ion [51]	Cu/Fe_2O_3, Cu_4/CF	Identified at above 250 °C
		CF	Anticipated to be identified at above 350 °C
1558	$(M-O)_2=NO$ [51]	Cu/Fe_2O_3, Cu_4/CF	Appear at above 300 °C
1246	$(M-O)_2=NO$ [51]	Cu/Fe_2O_3, Cu_4/CF	Increase
1374-1378	Free NO_3^- ion [51]	Cu/CeO_2	Increase slowly, stable, visible at all temperatures
1406	M-NO_2 [51]	Cu/CeO_2	Decrease, disappear at above 200 °C
1278	M-NO_2 [51]	Cu/CeO_2	Decrease, disappear at above 200 °C
1312	M-O-NO_2 [51]	Cu/CeO_2	Appear at 350 °C
1465	Monodentate carbonate, -CO_3^{2-} [24]	Cu/CeO_2	Appear at 150-200 °C, first increase, then decrease
1516–1524	Bidentate carbonate, -CO_3^{2-} [24]	Cu/CeO_2	Increase, then decrease slowly
1622–1575	Bidentate carbonate, -CO_3^{2-} [24]	Cu/CeO_2	Increase, then decrease slowly
1130	NO^{3-} [51]	Cu/Fe_2O_3, Cu_4/CF	Appear and increase at above 300 °C
1083	NO^{3-} [51]	Cu/Fe_2O_3, Cu_4/CF	The broad peak decreases at below 200 °C, and then becomes sharp and increase at above 250 °C
1030–1038	Cis-$N_2O_2^{2-}$, M-(ON = NO), ν_s(N-O) [51,52]	Cu/CeO_2, CF	Decrease slowly
830–833	Cis-$N_2O_2^{2-}$, M-(ON = NO), ν_{as}(N-O) [51,52]	All	Decrease

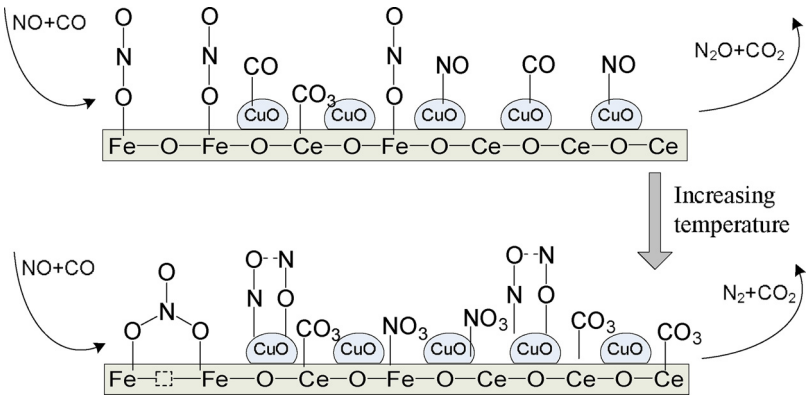

Fig. 11. Possible reaction mechanisms of NO reduction by CO over Cu/CF catalyst.

study was performed for NO + CO reaction with the spectra presented in Fig. 10. Table 5 summarizes the observed bands over each catalyst sample as well as their evolution behaviours and assignments. The assignment of the bands could be confirmed by the *in situ* DRIFT spectra of CO adsorption and NO + O_2 coadsorption provided in the supplementary information (section S5). For all the catalyst samples, the adsorbed NO_x species are mainly NO^+ at 2415 cm^{-1}, Cu^{2+}-NO at 2177 cm^{-1}, physical adsorbed NO at 2116 cm^{-1}, -$(NO)_2$ at 1843 and 1767 cm^{-1}, NONO at 1720–1625 cm^{-1}, M-NO_2 at 1392 and 1357 cm^{-1}, free nitrate ion NO_3^- at 1379 cm^{-1}, $(M-O)_2=NO$ at 1558 and 1246 cm^{-1}, and M−(ON=NO) at 1038 and 833 cm^{-1}. For Cu/CeO_2, bands of M−NO_2 at 1406 and 1278 cm^{-1}, and M−O−NO_2 at 1312 cm^{-1} could be observed. At lower temperatures, the adsorbed NO_x species are mainly −NO, −$(NO)_2$, M−NO_2, and M−(ON=NO),

where N has lower oxidation states. As the temperature is increased, these species decrease due to thermal desorption or reaction with CO. Some of them, especially M-NO_2, are further oxidized into nitrates, stored on the catalyst surface as free nitrate ion NO_3- or bridging nitrate $(M-O)_2$=NO.

The intensities of bands at 1400-1300 cm^{-1} over samples Cu/Fe_2O_3, CF, and Cu_4/CF are stronger than those over sample Cu/CeO_2, indicating that more nitrites and nitrates are stored over Fe_2O_3 support. Fe sites are speculated to be the storing sites of these NO_x species. The existence of Fe could help to anchor more nitrites and nitrates. Nitrites at 1399 and 1359 cm^{-1} are more stable over sample CF, which shows the worst catalytic performance, than those over other catalysts, implying that those stable nitrites are not the active intermediates for NO reduction. Another prominent difference of the evolution of NO_x species over sample CF is the absence of bridging nitrates and the strong ruffles of NONO at 1720–1625 cm^{-1}, which may be the active intermediates for NO + CO reaction. The impregnated copper may play an essential role in the conversion of inactive nitrites into active nitrates and other NO_x species.

CO is adsorbed on the catalyst surface as physical adsorbed CO at around 2170 cm^{-1} and over Cu^+ sites as Cu^+-CO at around 2110 cm^{-1}. Over Cu/CeO_2, peaks of physical adsorbed CO decrease very fast and disappear at 100 °C. Peaks of Cu^+-CO disappear at 150 °C due to the further reduction of Cu^+ to Cu0. The excellent reducibility of copper over CeO_2 support could result in its good activity toward CO oxidation. Bands of CO are much more stable over other samples, implying a worse catalytic activity of CO oxidation. The superior performance of CO oxidation over Cu/CeO_2 sample could also be confirmed by the significantly increase bands of CO_2 at higher temperatures. It could be concluded that the CeO_2 supported copper catalysts have much better performance for CO oxidation than Fe_2O_3 or CF supported catalysts. Fe incorporation could enhance the activity of CO + NO reaction, but the activity of CO oxidation is inhibited. At the same time, several bands of carbonate at 1620–1465 cm^{-1} could be observed over Cu/CeO_2 but not over other samples. CO tends to be adsorbed on the catalyst surface as carbonate more easily over CeO_2 rather than over Fe_2O_3 or Fe containing oxides (CF). The conclusion could be confirmed by the *in situ* DRIFT spectra of CO adsorption over different catalyst samples (section S5 of the supplementary information).

It could be concluded that CeO_2 could serve as the storing sites of carbonate and enhance CO oxidation, Fe_2O_3 could serve as the storing sites of nitrites and nitrates and facilitate NO_x adsorption, and impregnated copper could help to convert inactive nitrites into active intermediates nitrates and NONO for NO + CO reaction. The promoted adsorption and conversion of both carbonates and nitrite/nitrates over catalyst Cu/CF is expected to be the reason for its excellent catalytic activity for NO + CO reaction. The proposed reaction mechanism over catalyst Cu/CF is illustrated in Fig. 11.

4. Conclusion

The synthesised Cu/CF catalyst with mixed metal oxide support showed better catalytic activity for NO + CO reaction than those supported over single metal oxide, *i.e.*, Cu/Fe_2O_3 and Cu/CeO_2. The physical and chemical properties of Cu/CF catalyst were further investigated. TEM, XRD and Raman tests indicated that cubic CeO_2 may serve as the lattice framework in the mixed oxides cf. Fe_2O_3 phase are mainly formed on the surface of CeO_2 lattice in the CF involved samples, and these 'topped' Fe_2O_3 phase on the CeO_2 crystals may also facilitate the incorporation of iron atoms into CeO_2 lattice. XPS results further confirmed that Fe is incorporated into the CeO_2 lattice since the chemical state of Fe is altered by the CeO_2 lattice but the state of Ce is not influence by Fe. The high fraction of oxygen vacancy in catalyst Cu/CF may also facilitate the redox cycle of oxygen during catalytic reactions. H_2-TPR results illustrated that the interaction of Cu oxide with CF support favourably promoted the reduction of Cu oxide and diffusion of surface oxygen species at low temperatures.

In situ DRIFT study revealed that CeO_2 could serve as the storing sites of carbonate and enhance CO oxidation, Fe_2O_3 could serve as the storing sites of nitrites and nitrates and facilitate NOx adsorption, and impregnated copper could help to convert inactive nitrites into active intermediates nitrates and NONO for NO + CO reaction. The promoted adsorption and conversion of both carbonates and nitrite/nitrates over catalyst Cu/CF is expected to be the reason for its excellent catalytic activity for NO + CO reaction. The good catalytic activity of Cu/CF for NO + CO reaction implies its potential application in the rotary reactor [11], which was designed for treatment of flue gas from stationary sources. The performance of separated NOx adsorption-reduction process will be tested for modeled flue gas with moisture and excess oxygen in the future work.

Acknowledgements

The authors thankthe National Natural Science Foundation of China (NO. 51776113 and NO. 51776114), Natural Science Foundation of Shandong Province (NO. ZR2017MEE035), the Key R&D Program Funds of Shandong Province (NO. 2017GSF17122), and the Foundation of Shandong University for Young Scholar's Future Plan (NO. 2017WLJH29) for the financial support.

Appendix A. Supplementary data

Supplementary material related to this article can be found, in the online version, at doi:https://doi.org/10.1016/j.apcatb.2018.08.054.

References

[1] M. Pacella, A. Garbujo, J. Fabro, M. Guiotto, Q. Xin, M.M. Natile, P. Canu, P. Cool, A. Glisenti, PGM-free CuO/$LaCoO_3$ nanocomposites: new opportunities for TWC application, Appl. Catal. B-Environ. 227 (2018) 446–458.
[2] K. Huang, L.L. Lin, K. Yang, W.X. Dai, X. Chen, X.Z. Fu, Promotion effect of ultraviolet light on NO plus CO reaction over Pt/TiO_2 and Pt/CeO_2-TiO_2 catalysts, Appl. Catal. B-Environ. 179 (2015) 395–406.
[3] Y.J. Song, Y.M. Lopez-De Jesus, P.T. Fanson, C.T. Williams, Kinetic evaluation of direct NO decomposition and NO-CO reaction over dendrimer-derived bimetallic Ir-Au/Al_2O_3 catalysts, Appl. Catal. B-Environ. 154 (2014) 62–72.
[4] X.W. Wang, X.L. Wu, N. Maeda, A. Baiker, Striking activity enhancement of gold supported on Al-Ti mixed oxide by promotion with ceria in the reduction of NO with CO, Appl. Catal. B-Environ. 209 (2017) 62–68.
[5] X.X. Cheng, L.Y. Wang, Z.Q. Wang, M.Z. Zhang, C.Y. Ma, Catalytic performance of NO reduction by CO over activated semicoke supported Fe/Co catalysts, Ind. Eng. Chem. Res. 55 (50) (2016) 12710–12722.
[6] C.A. Sierra-Pereira, E.A. Urquieta-Gonzalez, Reduction of NO with CO on CuO or Fe_2O_3 catalysts supported on TiO_2 in the presence of O_2, SO_2 and water steam, Fuel 118 (2014) 137–147.
[7] I. Spassova, M. Khristova, D. Panayotov, D. Mehandjiev, Coprecipitated CuO-MnO_x catalysts for low-temperature CO-NO and CO-NO-O_2 reactions, J. Catal. 185 (1) (1999) 43–57.
[8] T. Yamamoto, T. Tanaka, S. Suzuki, R. Kuma, K. Teramura, Y. Kou, T. Funabiki, S. Yoshida, NO reduction with CO in the presence of O_2 over Cu/Al_2O_3 (3) structural analysis of active species by means of XAFS and UV/VIS/NIR spectroscopy, Top. Catal. 18 (1-2) (2002) 113–118.
[9] A.G. Makeev, N.V. Peskov, H. Yanagihara, Modeling of the catalytic removal of CO and NO under lean-burn conditions: can there be too much catalyst? Appl. Catal. B-Environ. 119 (2012) 273–278.
[10] Y. Wang, A.M. Zhu, Y.Z. Zhang, C.T. Au, X.F. Yang, C. Shi, Catalytic reduction of NO by CO over NiO/CeO2 catalyst in stoichiometric NO/CO and NO/CO/O_2 reaction, Appl. Catal. B-Environ. 81 (1-2) (2008) 141–149.
[11] X.X. Cheng, M. Zhang, P.L. Sun, L.Y. Wang, Z.Q. Wang, C.Y. Ma, Nitrogen oxides reduction by carbon monoxide over semi-coke supported catalysts in a simulated rotary reactor: reaction performance under dry conditions, Green Chem. 18 (19) (2016) 5305–5324.
[12] X.X. Cheng, X.Y. Zhang, M. Zhang, P.L. Sun, Z.Q. Wang, C.Y. Ma, A simulated rotary reactor for NOx reduction by carbon monoxide over Fe/ZSM-5 catalysts, Chem. Eng. J. 307 (2017) 24–40.
[13] L.H. Dong, L.L. Zhang, C.Z. Sun, W.J. Yu, J. Zhu, L.J. Liu, B. Liu, Y.H. Hu, F. Gao, L. Dong, Y. Chen, Study of the properties of CuO/VO_x/$Ti_{0.5}Sn_{0.5}O_2$ catalysts and their activities in NO plus CO reaction, ACS Catal. 1 (5) (2011) 468–480.
[14] I. Castellanos, O. Marie, Fe-HFER and Cu-HFER as catalysts for the NO_x SCR using acetylene as a reducing agent: reaction mechanism revealed by FT-IR operando study coupled with ^{15}N isotopic labelling, Appl Catal B-Environ 223 (2018)

143–153.
[15] S. Ali, L.Q. Chen, F.L. Yuan, R. Li, T.R. Zhang, S.U. Bakhtiar, X.S. Leng, X.Y. Niu, Y.J. Zhu, Synergistic effect between copper and cerium on the performance of Cu_x-$Ce_{0.5-x}$-$Zr_{0.5}$ (x = 0.1-0.5) oxides catalysts for selective catalytic reduction of NO with ammonia, Appl. Catal. B-Environ. 210 (2017) 223–234.
[16] L.L. Li, L. Zhang, K.L. Ma, W.X. Zou, Y. Cao, Y. Xiong, C.J. Tang, L. Dong, Ultra-low loading of copper modified TiO_2/CeO_2 catalysts for low-temperature selective catalytic reduction of NO by NH_3, Appl. Catal. B-Environ. 207 (2017) 366–375.
[17] G. Perin, J. Fabro, M. Guiotto, Q. Xin, M.M. Natile, P. Cool, P. Canu, A. Glisenti, Cu@$LaNiO_3$ based nanocomposites in TWC applications, Appl. Catal. B-Environ. 209 (2017) 214–227.
[18] L.H. Dong, B. Zhang, C.J. Tang, B. Li, L.Y. Zhou, F.Z. Gong, B.Z. Sun, F. Gao, L. Dong, Y. Chen, Influence of CeO_2 modification on the properties of Fe_2O_3-$Ti_{0.5}Sn_{0.5}O_2$ catalyst for NO reduction by CO, Catal. Sci. Technol. 4 (2) (2014) 482–493.
[19] J. Li, S. Wang, L. Zhou, G.H. Luo, F. Wei, NO reduction by CO over a Fe-based catalyst in FCC regenerator conditions, Chem. Eng. J. 255 (2014) 126–133.
[20] L.Y. Wang, X.X. Cheng, Z.Q. Wang, C.Y. Ma, Y.K. Qin, Investigation on Fe-Co binary metal oxides supported on activated semi-coke for NO reduction by CO, Appl. Catal. B-Environ. 201 (2017) 636–651.
[21] Y. Xin, N.N. Zhang, Q. Li, Z.L. Zhang, X.M. Cao, L.R. Zheng, Y.W. Zeng, J.A. Anderson, Selective catalytic reduction of NOx with NH_3 over short-range ordered W-O-Fe structures with high thermal stability, Appl. Catal. B-Environ. 229 (2018) 81–87.
[22] B. Li, Z.Y. Ren, Z.X. Ma, X.D. Huang, F. Liu, X.B. Zhang, H.S. Yang, Selective catalytic reduction of NO by NH_3 over CuO-CeO_2 in the presence of SO_2, Catal. Sci. Technol. 6 (6) (2016) 1719–1725.
[23] X.J. Yao, Q. Yu, Z.Y. Ji, Y.Y. Lv, Y. Cao, C.J. Tang, F. Gao, L. Dong, Y. Chen, A comparative study of different doped metal cations on the reduction, adsorption and activity of CuO/$Ce_{0.67}M_{0.33}O_2$ (M = Zr^{4+}, Sn^{4+}, Ti^{4+}) catalysts for NO plus CO reaction, Appl. Catal. B-Environ. 130 (2013) 293–304.
[24] X.J. Yao, Y. Xiong, J.F. Sun, F. Gao, Y. Deng, C.J. Tang, L. Dong, Influence of MnO_2 modification methods on the catalytic performance of CuO/CeO_2 for NO reduction by CO, J. Rare Earth 32 (2) (2014) 131–138.
[25] D. Gamarra, A.L. Camara, M. Monte, S.B. Rasmussen, L.E. Chinchilla, A.B. Hungria, G. Munuera, N. Gyorffy, Z. Schay, V.C. Corberan, J.C. Conesa, A. Martinez-Arias, Preferential oxidation of CO in excess H_2 over CuO/CeO_2 catalysts: characterization and performance as a function of the exposed face present in the CeO_2 support, Appl. Catal. B-Environ. 130 (2013) 224–238.
[26] L. Qi, Q. Yu, Y. Dai, C.J. Tang, L.J. Liv, H.L. Zhang, F. Gao, L. Dong, Y. Chen, Influence of cerium precursors on the structure and reducibility of mesoporous CuO-CeO_2 catalysts for CO oxidation, Appl. Catal. B-Environ. 119 (2012) 308–320.
[27] D. Delimaris, T. Ioannides, VOC oxidation over CuO-CeO_2 catalysts prepared by a combustion method, Appl. Catal. B-Environ. 89 (1-2) (2009) 295–302.
[28] K. Kamonsuangkasem, S. Therdthianwong, A. Therdthianwong, N. Thammajak, Remarkable activity and stability of Ni catalyst supported on CeO_2-Al_2O_3 via $CeAlO_3$ perovskite towards glycerol steam reforming for hydrogen production, Appl. Catal. B-Environ. 218 (2017) 650–663.
[29] Y.X. Wang, F. Kapteijn, M. Makkee, NOx reduction in the Di-air system over noble metal promoted ceria, Appl. Catal. B-Environ. 231 (2018) 200–212.
[30] L.J. Liu, B. Liu, L.H. Dong, J. Zhu, H.Q. Wan, K.Q. Sun, B. Zhao, H.Y. Zhu, L. Dong, Y. Chen, In situ FT-infrared investigation of CO or/and NO interaction with CuO/$Ce_{0.67}Zr_{0.33}O_2$ catalysts, Appl. Catal. B-Environ. 90 (3-4) (2009) 578–586.
[31] L.J. Liu, Z.J. Yao, B. Liu, L. Dong, Correlation of structural characteristics with catalytic performance of CuO/$Ce_xZr_{1-x}O_2$ catalysts for NO reduction by CO, J. Catal. 275 (1) (2010) 45–60.
[32] L.J. Liu, Y. Chen, L.H. Dong, J. Zhu, H.Q. Wan, B. Liu, B. Zhao, H.Y. Zhu, K.Q. Sun, L. Dong, Y. Chen, Investigation of the NO removal by CO on CuO-CoO_x binary metal oxides supported on $Ce_{0.67}Zr_{0.33}O_2$, Appl. Catal. B-Environ. 90 (1-2) (2009) 105–114.
[33] G. Landi, A. Di Benedetto, S. Colussi, P.S. Barbato, L. Lisi, Effect of carbon dioxide and water on the performances of an iron-promoted copper/ceria catalyst for CO preferential oxidation in H_2-rich streams, Int. J. Hydrogen Energy 41 (18) (2016) 7332–7341.
[34] J. Wang, C.Y. Han, X.Y. Gao, J.C. Lu, G.P. Wan, D.D. He, R. Chen, K.Z. Chen, S.F. He, Y.M. Luo, Rapid synthesis of Fe-doped CuO-$Ce_{0.8}Zro_{0.2}O_2$ catalysts for CO preferential oxidation in H_2-rich streams: effect of iron source and the ratio of Fe/Cu, J. Power Sources 343 (2017) 437–445.
[35] W.Y. Hernandez, M.A. Centeno, S. Ivanova, P. Eloy, E.M. Gaigneaux, J.A. Odriozola, Cu-modified cryptomelane oxide as active catalyst for CO oxidation reactions, Appl. Catal. B-Environ. 123 (2012) 27–35.
[36] A. Davo-Quinonero, D. Lozano-Castello, A. Bueno-Lopez, Unexpected stability of CuO/Cryptomelane catalyst under preferential oxidation of CO reaction conditions in the presence of CO_2 and H_2O, Appl. Catal. B-Environ. 217 (2017) 459–465.
[37] Z.L. Yuan, L.N. Wang, J.H. Wang, S.X. Xia, P. Chen, Z.Y. Hou, X.M. Zheng, Hydrogenolysis of glycerol over homogenously dispersed copper on solid base catalysts, Appl. Catal. B-Environ. 101 (3-4) (2011) 431–440.
[38] C.Z. Sun, J. Zhu, Y.Y. Lv, L. Qi, B. Liu, F. Gao, K.Q. Sun, L. Dong, Y. Chen, Dispersion, reduction and catalytic performance of CuO supported on ZrO_2-doped TiO_2 for NO removal by CO, Appl. Catal. B-Environ. 103 (1-2) (2011) 206–220.
[39] M. Lubbe, A.M. Gigler, R.W. Stark, W. Moritz, Identification of iron oxide phases in thin films grown on Al_2O_3(0001) by Raman spectroscopy and X-ray diffraction, Surf. Sci. 604 (7-8) (2010) 679–685.
[40] Y.-S. Li, J.S. Church, A.L. Woodhead, Infrared and Raman spectroscopic studies on iron oxide magnetic nano-particles and their surface modifications, J. Magn. Magn. Mater. 324 (2012) 1543–1550.
[41] L. Bellot-Gurlet, D. Neff, S. Reguer, J. Monnier, M. Saheb, P. Dillmann, Raman studies of corrosion layers formed on archaeological Irons in various media, J Nano Res.-Sw 8 (2009) 147–156.
[42] L.J. Liu, Z.J. Yao, Y. Deng, F. Gao, B. Liu, L. Dong, Morphology and crystal-plane effects of nanoscale ceria on the activity of CuO/CeO_2 for NO reduction by CO, Chemcatchem 3 (6) (2011) 978–989.
[43] L. Li, F. Chen, J.Q. Lu, M.F. Luo, Study of defect sites in $Ce_{1-x}M_xO_{2-d}$ (x = 0.2) solid solutions using Raman spectroscopy, J. Phys. Chem. A 115 (27) (2011) 7972–7977.
[44] Q. Yu, L.J. Liu, L.H. Dong, D. Li, B. Liu, F. Gao, K.Q. Sun, L. Dong, Y. Chen, Effects of Ce/Zr ratio on the reducibility, adsorption and catalytic activity of CuO/$CexZr_{1-x}O_2$/g-Al_2O_3 catalysts for NO reduction by CO, Appl. Catal. B-Environ. 96 (3-4) (2010) 350–360.
[45] T. Yamashita, P. Hayes, Analysis of XPS spectra of Fe^{2+} and Fe^{3+} ions in oxide materials, Appl. Surf. Sci. 254 (8) (2008) 2441–2449.
[46] X.J. Yao, Y. Xiong, W.X. Zou, L. Zhang, S.G. Wu, X. Dong, F. Gao, Y. Deng, C.J. Tang, Z. Chen, L. Dong, Y. Chen, Correlation between the physicochemical properties and catalytic performances of $Ce_xSn_{(1-x)}O_2$ mixed oxides for NO reduction by CO, Appl. Catal. B-Environ. 144 (2014) 152–165.
[47] Y.L. Zhang, L.L. Ma, T.J. Wang, X.J. Li, MnO_2 coated Fe_2O_3 spindles designed for production of C_{5+} hydrocarbons in Fischer-Tropsch synthesis, Fuel 177 (2016) 197–205.
[48] P. Ratnasamy, D. Srinivas, C.V.V. Satyanarayana, P. Manikandan, R.S.S. Kumaran, M. Sachin, V.N. Shetti, Influence of the support on the preferential oxidation of CO in hydrogen-rich steam reformates over the CuO-CeO_2-ZrO_2 system, J. Catal. 221 (2) (2004) 455–465.
[49] H. Zhou, Y.X. Su, W.Y. Liao, W.Y. Deng, F.C. Zhong, NO reduction by propane over monolithic cordierite-based Fe/Al_2O_3 catalyst: reaction mechanism and effect of H_2O/SO_2, Fuel 182 (2016) 352–360.
[50] C.X. Wang, W.Z. Xia, Y.K. Zhao, New insight into hydroxyl-mediated NH_3 formation on the Rh-CeO_2 catalyst surface during catalytic reduction of NO by CO, Chin. J. Catal. 38 (8) (2017) 1399–1405.
[51] K.I. Hadjiivanov, Identification of neutral and charged N_xO_y surface species by IR spectroscopy, Catal. Rev. 42 (1-2) (2000) 71–144.
[52] M. Konsolakis, Comments regarding DRIFTS data interpretation on "Effect of CeO_2 addition to Rh/Al_2O_3 catalyst on N2O decomposition" by SS Kim, SJ Lee, SC Hong in Chem. Eng. J. 169 (2011) 173, Chem. Eng. J. 183 (2012) 550–551.